



THE UNIVERSITY *of* EDINBURGH

Edinburgh Research Explorer

## Physical-Layer Security in Multiuser Visible Light Communication Networks

### Citation for published version:

Yin, L & Haas, H 2017, 'Physical-Layer Security in Multiuser Visible Light Communication Networks', *IEEE Journal on Selected Areas in Communications*, pp. 162 - 174. <https://doi.org/10.1109/JSAC.2017.2774429>

### Digital Object Identifier (DOI):

[10.1109/JSAC.2017.2774429](https://doi.org/10.1109/JSAC.2017.2774429)

### Link:

[Link to publication record in Edinburgh Research Explorer](#)

### Document Version:

Peer reviewed version

### Published In:

IEEE Journal on Selected Areas in Communications

### General rights

Copyright for the publications made accessible via the Edinburgh Research Explorer is retained by the author(s) and / or other copyright owners and it is a condition of accessing these publications that users recognise and abide by the legal requirements associated with these rights.

### Take down policy

The University of Edinburgh has made every reasonable effort to ensure that Edinburgh Research Explorer content complies with UK legislation. If you believe that the public display of this file breaches copyright please contact [openaccess@ed.ac.uk](mailto:openaccess@ed.ac.uk) providing details, and we will remove access to the work immediately and investigate your claim.



# Physical-Layer Security in Multiuser Visible Light Communication Networks

Liang Yin and Harald Haas, *Senior Member, IEEE*

**Abstract**—In this paper, we study the physical-layer security in a 3-D multiuser visible light communication (VLC) network. The locations of access points (APs) and mobile users are modeled as two 2-D, independent and homogeneous Poisson point processes at distinct heights. Using mathematical tools from stochastic geometry, we provide a new analytical framework to characterize the secrecy performance in multiuser VLC networks. Closed-form results for the outage probability and the ergodic secrecy rate are derived for networks without AP cooperation. Considering the cooperation among APs, we give tight lower and upper bounds on the secrecy outage probability and the ergodic secrecy rate. To further enhance the secrecy performance at the legitimate user, a disk-shaped secrecy protected zone is implemented in the vicinity of the transmit AP. Based on the obtained results, it is shown that cooperating neighboring APs in a multiuser VLC network can bring performance gains on the secrecy rate, but only to a limited extent. We also show that building an eavesdropper-free protected zone around the AP significantly improves the secrecy performance of legitimate users, which appears to be a promising solution for the design of multiuser VLC networks with high security requirements.

**Index Terms**—Visible light communication, secrecy capacity, physical-layer security, poisson point process, stochastic geometry.

## I. INTRODUCTION

BY UTILIZING the existing lighting infrastructure and shifting the communication frequency to the visible spectrum, visible light communication (VLC) [1]–[3] has recently emerged as a promising candidate for future high-speed broadband communications, which could effectively alleviate the spectrum congestion issue in current radio frequency (RF) based wireless systems. Recent advances have also led to the standardization of short-range wireless optical communication using VLC for local and metropolitan area networks [4], which serves as a major step towards its commercialization in the near future. Compared to RF communication, VLC has the following main advantages: 1) VLC builds upon existing lighting devices and operates on the license-free spectrum so that it has lower implementation cost; 2) VLC can operate safely in electromagnetic sensitive areas, where RF is intrinsically prohibited; 3) VLC networking can be designed in

addition to existing heterogeneous wireless networks because it receives zero interference from, and adds zero interference to its RF counterparts; 4) Based on the property that visible light does not penetrate through opaque objects, the communication bandwidth in one room can be efficiently reused in other rooms to obtain a high frequency reuse factor and hence a high area spectral efficiency; 5) Indoor VLC typically achieves higher physical-layer security since the transmitted signal is confined within the room.

The broadcast property of VLC has been utilized in many novel designs of multiuser VLC networks [5]–[7]. However, it also causes potential concerns to legitimate users and network administrators regarding the information privacy and confidentiality, especially in public areas, such as train stations and libraries. From an information-theoretic point of view, the physical-layer security was pioneered by Wyner for proposing the wiretap channel [8]: a channel in which an eavesdropper receives a degraded version of the transmitted signal. The degraded wiretap channel was later extended to the non-degraded broadcast channel by Csiszár and Körner [9]. In their seminal work, it is shown that perfect secrecy can be achieved as long as the legitimate user has a less degraded channel than the eavesdropper, and the secrecy capacity is derived as the difference between the information capacity for the two users. Typical security enhancement techniques that are implemented at upper layers of the communication chain include password protection and user admission control. Physical-layer security, on the other hand, exploits the randomness of the noise and the wireless communication channel to limit the amount of legitimate information to be detected by unauthorized eavesdroppers [8], [9].

Different from point-to-point communication, studying the secrecy performance in a large-scale wireless network requires not only the knowledge of locations of legitimate users but also the knowledge of locations of eavesdropping users that may interact with legitimate users. Initial works that characterize the secrecy performance in multiuser wireless networks rely on the secrecy graph model to study the node connectivity [10], [11] and the maximum secrecy rate [12], from an information-theoretic perspective. Following these works, the secrecy rate per source-destination pair was investigated in [13] by characterizing the secrecy capacity scaling laws in a wireless network. Moving from network information theory, recent works have evaluated the secrecy performance in multiuser wireless networks using mathematical tools from stochastic geometry [14], [15]. It should be noted that works in [8]–[15] are all focused on RF based wireless networks.

Manuscript received February 22, 2017; revised July 15, 2017; accepted September 16, 2017. This work was supported by the U.K. Engineering and Physical Sciences Research Council under Grant EP/K008757/1. (Corresponding author: Liang Yin.)

The authors are with the School of Engineering, Institute for Digital Communications, Li-Fi Research and Development Centre, University of Edinburgh, Edinburgh EH9 3JL, U.K. (e-mail: l.yin@ed.ac.uk; h.haas@ed.ac.uk).

Color versions of one or more of the figures in this paper are available online at <http://ieeexplore.ieee.org>.

Digital Object Identifier 10.1109/JSAC.2017.2774429

Different from RF communication, which is typically modeled as a Gaussian broadcast channel with an average power constraint at the transmitter side, VLC typically uses intensity modulation and direct detection (IM/DD) due to the use of inexpensive light-emitting diodes (LEDs) and photodiodes (PDs) as the optical transmitter and receiver, respectively. In VLC, since the signal is modulated onto the intensity of the emitted light, it must satisfy average, peak as well as non-negative amplitude constraints, that are imposed by the dynamic range of typical LEDs and practical illumination requirements [6], [16]–[18]. Although typical LEDs have a nonlinear electrical-to-optical (E/O) transfer characteristic, this nonlinearity can be successfully compensated by pre-distortion techniques [19]. Also, since the wavelength of visible light is hundreds of nanometers while the detection area of a typical PD is millions of square wavelengths, this spatial diversity essentially prevents the “multipath fading” effect in the VLC channel. Due to these fundamental differences, results on the secrecy capacity obtained for RF networks can not be directly applied to VLC networks.

Since the secrecy capacity is related to the information capacity of the communication channel [8], [9], before determining the secrecy capacity in VLC networks it is essential to obtain the information capacity of the VLC channel with average, peak and non-negative constraints. However, to the best of authors’ knowledge, the exact information capacity of the VLC channel with such constraints still remains unknown, even for the simplest single-input single-output (SISO) case, despite some lower and upper bounds have been derived [16]–[18]. By considering one transmitter, one legitimate user and one eavesdropper in a VLC system, lower and upper bounds on the secrecy capacity of the amplitude-constrained Gaussian wiretap channel was recently studied in [20], with the use of the derived capacity lower and upper bounds in [16]. In the same work [20], beamforming was also utilized to improve the secrecy capacity for the multiple-input single-output (MISO) VLC channel. Following this, the optimal beamformer design problem subject to amplitude constraints was further studied in [21]. The secrecy performance in a single-cell VLC system with only one AP was studied in [22]. However, the randomness of legitimate users as well as eavesdroppers and, more importantly, the interactions between them, have not been fully characterized when analyzing the secrecy performance in a random multiuser VLC network.

### A. Approaches and Contributions

In this work, we aim to characterize the secrecy performance in an indoor multiuser VLC network by considering the unique properties of the VLC channel as well as the network layout, that differ from typical RF networks. Our approach builds upon a proposed three-dimensional network model with two independent random topologies for the VLC APs and mobile users. Specifically, the VLC APs are modeled by a two-dimensional homogeneous Poisson point process (PPP) in the ceiling, while the locations of users, that include both legitimate users and eavesdroppers, are modeled by another independent two-dimensional homogeneous PPP at

the user plane. To separate eavesdroppers from legitimate users, the locations of random eavesdroppers are obtained from a thinned PPP. Despite the grid-like deployment of LEDs in typical offices, the following observations indicate that a stochastic model may be required to accurately capture the distribution of APs in a VLC network. First, more and more LEDs with built-in motion-detection sensors are deployed in public spaces in order to reduce energy consumption. In this case, some of the LEDs will be temporally switched off when they are not required to provide illumination. Second, the distribution of ceiling lights is not necessarily equivalent to the distribution of APs in a VLC network because not necessarily all of the ceiling lights are simultaneously operating in the communication mode, i.e., some of the ceiling lights may operate in the illumination mode only when no data traffic is demanded from them. In these scenarios, the distribution of APs can not be accurately modeled by the grid model. Instead, a stochastic thinning process built upon the grid-like deployment of LEDs is more accurate, where the activeness/idleness of each AP is determined by a time-varying probability distribution function (PDF). However, finding the PDF of activeness/idleness of the LED requires full knowledge of the users’ movement and handover characteristics, which is generally complicated and not analytically tractable. In order to derive analytically tractable results, the PPP model is assumed in this work. For completeness, we also compare the secrecy performance between the PPP model and the grid model and provide a method of applying the derived analytical results to estimate the secrecy performance in a conventional grid-like VLC network.

The main contributions of this paper are as follows:

- 1) When the legitimate user is served by the nearest AP in its vicinity, we derive the distribution function of the secrecy rate of a typical legitimate user, based on which secrecy outage probability and ergodic secrecy rate are obtained. To provide further insights into the secrecy performance with different network parameters, lower and upper bounds on the secrecy outage probability as well as on the ergodic secrecy rate are given.
- 2) We enhance the secrecy performance by implementing AP cooperation in a multiuser VLC network, and give lower and upper bounds on the secrecy outage probability and the ergodic secrecy rate. The derived analytical bounds are found to be reasonably tight in general and become tighter when the density of eavesdroppers becomes larger.
- 3) To further enhance the secrecy performance for legitimate users, we introduce a disk-shaped secrecy protected zone around the AP in a multiuser VLC network, in which the presence of eavesdroppers is prohibited. In this scenario, the secrecy outage probability and the ergodic secrecy rate are derived. The impact of designing the protected zone with different sizes on the secrecy performance is also investigated.

The remainder of this paper is organized as follows. In Section II, we introduce a three-dimensional link model for multiuser VLC networks and formulate the information-theoretic secrecy rate expression based on a close

203 approximation of the channel capacity. The secrecy outage  
 204 probability and the ergodic secrecy rate with/without the AP  
 205 cooperation are derived in Section III. We extend the analysis  
 206 on the secrecy performance in Section IV by implementing a  
 207 disk-shaped protected zone. Simulation results and discussions  
 208 are provided in Section V. Finally, concluding remarks are  
 209 given in Section VI.

## 210 II. SYSTEM MODEL

### 211 A. Poisson Network Model

212 We consider a downlink transmission scenario of a multiuser  
 213 VLC network with the presence of both legitimate users and  
 214 eavesdroppers inside a three-dimensional space. The VLC  
 215 APs are vertically fixed, since they are attached to the room  
 216 ceiling, and their horizontal positions are modeled by a  
 217 two-dimensional homogeneous PPP  $\Phi_a$  with density  $\lambda_a$ ,  
 218 in nodes per unit area. Similarly, mobile users are assumed to  
 219 be at a fixed height and their horizontal positions are modeled  
 220 by another independent two-dimensional homogeneous PPP  
 221  $\Phi_u$  with density  $\lambda_u$ . The vertical distance between the AP  
 222 plane and the user plane is denoted by  $L$ . After adding an  
 223 additional user at the room center,<sup>1</sup> the new point process  
 224 for mobile users becomes  $\Phi_u \cup \{0\}$ . Slivnyak's theorem states  
 225 that adding a user into  $\Phi_u$  is equivalent to conditioning  $\Phi_u$   
 226 on the added point, and this process does not change the  
 227 distribution of  $\Phi_u$  [23]. Therefore, the added user at the origin  
 228 can be treated as the *typical* legitimate user in the study  
 229 since it can reflect the spatial average of the performance of  
 230 all legitimate users in the network. Among all of the users,  
 231 there exist malicious eavesdroppers that could compromise  
 232 the transmission privacy of ongoing legitimate links, due to  
 233 the broadcast nature of the VLC channel. Since eavesdroppers  
 234 typically disguise as legitimate users, it is uncertain whether  
 235 a random user  $u \in \Phi_u$  is a legitimate user or an eavesdropper.  
 236 Therefore, it is assumed that  $u$  is an eavesdropper with  
 237 probability  $p_e$  and that  $u$  is a legitimate user with probability  
 238  $1 - p_e$ . This thinned realization of  $\Phi_u$  gives the point process  
 239 for eavesdroppers,  $\Phi_e$ , which is also a homogeneous PPP  
 240 whose density can be found as  $\lambda_e = p_e \lambda_u$  [23]. Furthermore,  
 241 it is assumed that eavesdroppers do not collude with each other  
 242 so that each eavesdropper needs to decode any confidential  
 243 messages sent to legitimate users individually. An example of  
 244 the described multiuser VLC network is depicted in Fig. 1.

245 A complete VLC channel includes both the line-of-  
 246 sight (LOS) link and non-line-of-sight (NLOS) links, that are  
 247 caused by light reflections from interior surfaces. However,  
 248 in a typical indoor lighting environment, the sum signal power  
 249 carried by NLOS components is significantly weaker than that  
 250 carried by the LOS link [1], [24], [25]. Therefore, we will  
 251 only focus on the LOS link in the following analysis in  
 252 order to obtain tractable analytical results. The VLC APs  
 253 are assumed to have a Lambertian radiation profile whose  
 254 Lambertian order is  $m = -1/\log_2(\cos(\Phi_{1/2}))$ , where  $\Phi_{1/2}$

<sup>1</sup>The room center is also called the origin. We use both expressions inter-  
 changeably throughout the paper since the room center has more geographical  
 meanings while the origin has more mathematical meanings when we apply  
 stochastic geometry tools in the theoretical analysis.

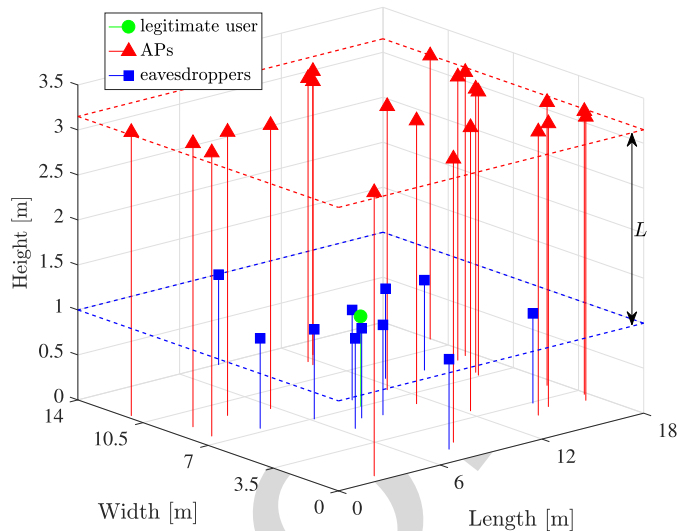


Fig. 1. Random network model: the legitimate user of interest is placed at the room center; VLC APs are randomly distributed in the ceiling according to a homogeneous PPP  $\Phi_a$ ; and eavesdroppers are randomly distributed on the same plane as the legitimate user, following a homogeneous PPP  $\Phi_e$ . In this example, an indoor VLC network of size  $18 \times 14 \times 3.5$  m<sup>3</sup> is shown.

255 denotes the semi-angle of the LED. The PD equipped at each  
 256 user is assumed to be facing vertically upwards with a field-of-  
 257 view (FOV) of  $\Psi_{\text{fov}}$ . For each VLC link, the optical channel  
 258 direct current (DC) gain is given by [26]:

$$259 \quad h = \frac{(m+1)A\eta}{2\pi d^2} \cos^m(\phi) T(\psi) g(\psi) \cos(\psi), \quad (1)$$

260 where  $A$  denotes the effective detection area of the PD;  $\eta$   
 261 is the responsivity of the PD;  $\phi$  and  $\psi$  are the angle of  
 262 irradiance and the angle of incidence of the optical link,  
 263 respectively;  $T(\psi)$  represents the gain of the optical filter used  
 264 at the receiver; and  $g(\psi)$  represents the gain of the optical  
 265 concentrator. The optical concentrator gain is given by [26]:

$$266 \quad g(\psi) = \begin{cases} \frac{n^2}{\sin^2(\Psi_{\text{fov}})}, & 0 \leq \psi \leq \Psi_{\text{fov}} \\ 0, & \psi > \Psi_{\text{fov}} \end{cases}, \quad (2)$$

267 where  $n$  is the reflective index of the optical concentrator, and  
 268 it is defined as the ratio of the speed of light in vacuum and  
 269 the phase velocity of light in the optical material. For visible  
 270 light, the typical value for  $n$  varies between 1 and 2.

271 Consider the communication link from an AP  $x \in \Phi_a$  to  
 272 an eavesdropper  $e \in \Phi_e$ . Based on the geometry [7] of the  
 273 VLC link, it is easy to obtain  $d = \sqrt{\|e - x\|^2 + L^2}$ ,  $\cos(\phi) =$   
 274  $L/\sqrt{\|e - x\|^2 + L^2}$  and  $\cos(\psi) = L/\sqrt{\|e - x\|^2 + L^2}$ .  
 275 Therefore, the received optical power at eavesdropper  $e$  from  
 276 AP  $x$  can be written as:

$$277 \quad P_{\text{rx}}(x, e) = h P_{\text{tx}} \\ 278 \quad = \frac{(m+1)A\eta T(\psi) g(\psi) L^{m+1}}{2\pi (\|e - x\|^2 + L^2)^{\frac{m+3}{2}}} P_{\text{tx}}, \quad (3)$$

279 where  $P_{\text{tx}}$  denotes the transmit optical power of the AP.  
 280 Similarly, the received signal power at the legitimate user can  
 281 be written as  $P_{\text{rx}}(x, o)$ , where  $o$  representing the origin is the  
 282 location of the typical user of interest.

### B. Secrecy Capacity Formulation

The classic Shannon equation does not apply to VLC because of the average, peak and non-negative constraints on the modulated optical signal. Although the exact capacity of the VLC channel remains unknown, several upper and lower bounds have been derived [16]–[18]. Based on the capacity lower bound derived in [16], the exact channel capacity of VLC can be written as:

$$C = \frac{1}{2} \log_2 \left( 1 + \frac{\exp(1)P_{\text{rx}}^2}{2\pi\sigma_n^2} \right) + \epsilon \left( \frac{P_{\text{rx}}}{\sigma_n} \right), \quad (4)$$

where  $\epsilon$ , as a function of the received optical-signal-to-noise ratio (OSNR)  $P_{\text{rx}}/\sigma_n$ , represents a positive capacity gap between the exact channel capacity and the analytical lower bound [16], and  $\sigma_n^2$  represents the total power of noise processes at the receiver. Note that inside the receiver circuit the dominant noise sources are the thermal noise and shot noise [1], [25]. The thermal noise is mainly caused by the preamplifier circuits while the shot noise originates mainly from the ambient light and/or other light sources. The signal-dependent shot noise, on the other hand, is relatively small, and hence its effect can be ignored. The overall noise process is generally well modeled as the additive white Gaussian noise (AWGN) [1], [25]. As the legitimate user and eavesdroppers may use different grades of receivers, for example, PDs with different detection areas and/or bandwidths, they are subject to different levels of receiver noise and are capable of detecting signals with different amplifying gains. Without loss of generality, the choice of different grades of receivers can be accounted for in the system model by assigning different noise variances at the legitimate user and the eavesdropper. Based on this, we denote by  $\sigma_{\text{nb}}^2$  and  $\sigma_{\text{ne}}^2$  the noise variance at the legitimate user and the noise variance at the eavesdropper, respectively. Unlike RF channels whose input signals are subject to an average power constraint [29], VLC channels require the input signals to satisfy a peak amplitude (optical power) constraint. This makes it challenging to obtain closed-form expressions for the secrecy capacity of a VLC link, even for the simplest SISO case [20], [30]. Therefore, in the following analysis we focus on a tight achievable lower bound on the secrecy capacity [20]:

$$C_s \geq [C_b - C_e]^+ = \underline{C}_s, \quad (5)$$

where  $[a]^+ = \max\{a, 0\}$ ;  $C_s$  represents the exact secrecy capacity;  $\underline{C}_s$  represents the tight lower bound on the secrecy capacity given by the right-hand side of (5);  $C_b$  is the channel capacity of the legitimate link; and  $C_e$  is the channel capacity of the eavesdropper's link.

### III. SECRECY RATE IN RANDOM VLC NETWORKS

#### A. Nearest AP to Serve the Legitimate User

Without AP cooperation, the nearest AP is typically assumed to serve a mobile user in the VLC network in order to maximize the information rate of the communication link. As a result, based on (4), the capacity of the legitimate link can be written as  $C_b = \max_{x \in \Phi_a} \frac{1}{2} \log_2(1 + \exp(1)P_{\text{rx}}^2(x, o)/2\pi\sigma_{\text{nb}}^2) + \epsilon(P_{\text{rx}}(x, o)/\sigma_{\text{nb}}) = \frac{1}{2} \log_2(1 + \exp(1)P_{\text{rx}}^2(x_0, o)/2\pi\sigma_{\text{nb}}^2) + \epsilon(P_{\text{rx}}(x_0, o)/\sigma_{\text{nb}})$ , where  $x_0$  represents the location of the

nearest AP to the origin. Since it is assumed that eavesdroppers do not collude, the secrecy performance of the legitimate user is limited by the eavesdropper with the highest OSNR. Therefore, the lower bound on the secrecy capacity at the typical legitimate user is formulated as:

$$\underline{C}_s = \left[ \frac{1}{2} \log_2 \left( 1 + \frac{\exp(1)P_{\text{rx}}^2(x_0, o)}{2\pi\sigma_{\text{nb}}^2} \right) - \frac{1}{2} \log_2 \left( 1 + \frac{\exp(1)P_{\text{rx}}^2(x_0, e^*(x_0))}{2\pi\sigma_{\text{ne}}^2} \right) + \epsilon \left( \frac{P_{\text{rx}}(x_0, o)}{\sigma_{\text{nb}}} \right) - \epsilon \left( \frac{P_{\text{rx}}(x_0, e^*(x_0))}{\sigma_{\text{ne}}} \right) \right]^+, \quad (6)$$

where  $e^*(x_0)$  denotes the horizontal distance from AP  $x_0$  to the nearest eavesdropper. Given that the legitimate user is connected to AP  $x$ , the general solution for  $e^*(x)$ , denoting the horizontal distance between AP  $x$  and the strongest eavesdropper, can be obtained by finding the location of the eavesdropper  $e \in \Phi_e$  that receives the strongest signal power:

$$\begin{aligned} e^*(x) &= \arg \max_{e \in \Phi_e} P_{\text{rx}}(x, e) \\ &= \arg \min_{e \in \Phi_e} \|e - x\|, \end{aligned} \quad (7)$$

where the last step is obtained based on the monotonic property of (3). By utilizing fractional frequency reuse [28] or orthogonal multiple access techniques, the achievable data rate can be quantified through the received signal-to-noise ratio (SNR) without the side effect of co-channel interference (CSI). As a result, OSNR of  $P_{\text{rx}}/\sigma_n > 30$  dB can be achieved at typical illumination levels [25], [27], where  $\epsilon(P_{\text{rx}}/\sigma_n)$  is found to be comparatively small [16]–[18]. Therefore, we focus on the high OSNR regime, where  $\epsilon(P_{\text{rx}}(x_0, o)/\sigma_{\text{nb}}) \ll 1/2 \log_2(\exp(1)P_{\text{rx}}^2(x_0, o)/2\pi\sigma_{\text{nb}}^2)$  and  $\epsilon(P_{\text{rx}}(x_0, e^*(x_0))/\sigma_{\text{ne}}) \ll 1/2 \log_2(\exp(1)P_{\text{rx}}^2(x_0, e^*(x_0))/2\pi\sigma_{\text{ne}}^2)$ . Based on this, (6) can be further approximated to:

$$\underline{C}_s \approx \left[ \frac{1}{2} \log_2 \left( \frac{P_{\text{rx}}^2(x_0, o)}{P_{\text{rx}}^2(x_0, e^*(x))} \right) + \log_2 \left( \frac{\sigma_{\text{ne}}}{\sigma_{\text{nb}}} \right) \right]^+ = R_s. \quad (8)$$

To distinguish from the exact secrecy capacity, we define in (8)  $R_s$  as the achievable secrecy rate. Due to the lack of the complete knowledge of the exact secrecy capacity  $C_s$ , the secrecy rate  $R_s$  is of interest in this paper. It is shown in (8) that a non-negative secrecy rate can only be achieved when the legitimate user achieves a higher SNR than the strongest eavesdropper. In the case that a eavesdropper receives signals from a less-degraded link than the legitimate user, the achievable secrecy rate drops to zero. It can also be seen from (8) that when the legitimate user and the eavesdropper use different grades of receivers, the achieved secrecy capacity at the legitimate user is offset by a constant, whose value is proportional to the logarithm of  $\sigma_{\text{ne}}/\sigma_{\text{nb}}$ . Therefore, without loss of generality,  $\sigma_{\text{nb}} = \sigma_{\text{ne}}$  is assumed in the following analysis.

*Theorem 1:* When the legitimate user is served by the nearest AP in its vicinity, the cumulative distribution function (CDF) of the secrecy rate  $R_s$  is given by:

$$F_{R_s}(v) = 1 - \frac{1}{1 + \frac{\lambda_e}{\lambda_a} 4^{\frac{v}{m+3}}} \exp\left(-\pi \lambda_e \left(4^{\frac{v}{m+3}} - 1\right) L^2\right), \quad (9)$$

where  $v \geq 0$ .

*Proof:* According to (8), we have  $R_s \geq 0$ . Therefore, the CDF of the secrecy rate  $R_s$  can be calculated by:

$$\begin{aligned} F_{R_s}(v) &= \mathbb{P}[R_s \leq v] \\ &= \mathbb{P}\left[\frac{P_{rx}^2(x_0, o)}{P_{rx}^2(x_0, e^*(x_0))} \leq 4^v\right] \\ &= \mathbb{P}\left[\|e^*(x_0) - x_0\| \leq \sqrt{\beta x_0^2 + (\beta - 1)L^2}\right], \end{aligned} \quad (10)$$

where  $\beta = 4^{v/(m+3)}$ . Since the legitimate user is served by the nearest AP, the PDF of  $x_0$  is [31]:

$$f_{x_0}(x_0) = 2\pi \lambda_a x_0 \exp\left(-\pi \lambda_a x_0^2\right). \quad (11)$$

When conditioned on distance  $x_0$ , (10) is the probability that no eavesdroppers exist within a circle, which is centered at  $x_0$  and has a radius of  $\sqrt{\beta x_0^2 + (\beta - 1)L^2}$ . Such probability can be calculated using the void probability of PPP [32]. As a result, (10) can be calculated as:

$$\begin{aligned} F_{R_s}(v) &= \mathbb{E}_{x_0} \left[ \mathbb{P} \left[ \|e^*(x_0) - x_0\| \leq \sqrt{\beta x_0^2 + (\beta - 1)L^2} \mid x_0 \right] \right] \\ &= \int_0^\infty \mathbb{P} \left[ \|e^*(x_0) - x_0\| \leq \sqrt{\beta x_0^2 + (\beta - 1)L^2} \mid x_0 \right] f_{x_0}(x_0) dx_0 \\ &= \int_0^\infty \left( 1 - \exp\left(-\pi \lambda_e \left(\beta x_0^2 + (\beta - 1)L^2\right)\right) \right) 2\pi \lambda_a x_0 \\ &\quad \times \exp\left(-\pi \lambda_a x_0^2\right) dx_0 \\ &= 1 - \frac{1}{1 + \frac{\lambda_e}{\lambda_a} \beta} \exp\left(-\pi \lambda_e (\beta - 1) L^2\right). \end{aligned} \quad (12)$$

After plugging  $\beta = 4^{v/(m+3)}$  into (12), we obtain (9). ■

*Corollary 1:* When the legitimate user is served by the  $n$ -th nearest AP in its vicinity, the CDF of the secrecy rate is:

$$F_{R_s}(v) = 1 - \left( \frac{1}{1 + \frac{\lambda_e}{\lambda_a} 4^{\frac{v}{m+3}}} \right)^n \exp\left(-\pi \lambda_e \left(4^{\frac{v}{m+3}} - 1\right) L^2\right), \quad (13)$$

where  $v \geq 0$ .

*Proof:* The distance distribution of the legitimate user to the  $n$ -th nearest AP is given by [31]:

$$f_{x_n}(x_n) = \frac{2(\pi \lambda_a x_n^2)^n}{x_n \Gamma(n)} \exp\left(-\pi \lambda_a x_n^2\right). \quad (14)$$

By using (14) and following similar steps as in (12), (13) can be obtained. ■

The secrecy outage probability, denoted by  $p_{so}$ , is defined as the probability that the secrecy rate is below a target secrecy rate  $\bar{R}_s$ . Mathematically, it is formulated as:

$$p_{so} = \mathbb{P}[R_s \leq \bar{R}_s] = F_{R_s}(\bar{R}_s), \quad (15)$$

which can be obtained directly from Theorem 1.

*Corollary 2:* When the legitimate user is served by the nearest AP in its vicinity, the secrecy outage probability is lower bounded by:

$$p_{so}^{LB} = 1 - \exp\left(-\pi \lambda_e \left(4^{\frac{\bar{R}_s}{m+3}} - 1\right) L^2\right), \quad (16)$$

when the density of VLC APs approaches infinity.

*Proof:* (16) can be obtained from  $p_{so}^{LB} = \lim_{\lambda_a \rightarrow \infty} p_{so}$ . ■

Theorem 1 and Corollary 2 provide an important guideline for the design of VLC networks: installing more VLC APs can help decrease the secrecy outage probability of a typical legitimate user; however, when the density of APs reaches a certain level, further increasing the density of APs is not meaningful since it can no longer enhance the secrecy performance. In other words, it is impossible for a legitimate user in the network to simultaneously achieve a target secrecy rate  $\bar{R}_s$  and have an outage probability lower than  $p_{so}^{LB}(\bar{R}_s)$ . Given a target secrecy rate  $\bar{R}_s$  and a target outage probability  $\bar{p}_{so} > p_{so}^{LB}(\bar{R}_s)$ , this requirement can be achieved by installing more APs in the network so that the density of APs satisfies  $\lambda_a \geq \lambda_e (1 - \bar{p}_{so}) 4^{\bar{R}_s/(m+3)} / (\bar{p}_{so} - p_{so}^{LB}(\bar{R}_s))$ . From (9) and (16), it is shown that reducing the semi-angle of the LED, or equivalently increasing the Lambertian order, can also help improve the secrecy performance of the network. Nevertheless, the actual choice of the semi-angle of the LED should also satisfy the illumination requirement.

*Theorem 2:* When the legitimate user is served by the nearest AP in its vicinity, the ergodic secrecy rate at the legitimate user is:

$$\begin{aligned} \mathbb{E}[R_s] &= \frac{m+3}{\ln(4)} \left[ \exp\left(\pi(\lambda_e + \lambda_a)L^2\right) \text{Ei}\left(-\pi(\lambda_e + \lambda_a)L^2\right) \right. \\ &\quad \left. - \exp\left(\pi\lambda_e L^2\right) \text{Ei}\left(-\pi\lambda_e L^2\right) \right], \end{aligned} \quad (17)$$

where  $\text{Ei}(a) = -\int_{-a}^\infty \exp(-t)/t dt$  is the exponential integral function [33].

*Proof:* The ergodic secrecy rate can be calculated based on the CDF of  $R_s$ :

$$\begin{aligned} \mathbb{E}[R_s] &= \int_0^\infty (1 - F_{R_s}(v)) dv \\ &= \frac{m+3}{\ln(4)} \int_1^\infty \frac{1}{\beta \left(1 + \frac{\lambda_e}{\lambda_a} \beta\right)} \exp\left(-\pi \lambda_e (\beta - 1) L^2\right) d\beta \\ &= \frac{m+3}{\ln(4)} \left[ \int_1^\infty \frac{\exp\left(-\pi \lambda_e (\beta - 1) L^2\right)}{\beta} d\beta \right. \\ &\quad \left. - \int_1^\infty \frac{\exp\left(-\pi \lambda_e (\beta - 1) L^2\right)}{\beta + \frac{\lambda_e}{\lambda_a}} d\beta \right], \end{aligned} \quad (18)$$

where the integration variable has been changed from  $v$  to  $\beta$ . After applying [33, eq. 3.351.5], the first integration in (18) can be calculated as:

$$\int_1^\infty \frac{\exp\left(-\pi \lambda_e (\beta - 1) L^2\right)}{\beta} d\beta = -\exp\left(\pi \lambda_e L^2\right) \text{Ei}\left(-\pi \lambda_e L^2\right). \quad (19)$$

After applying [33, eq. 3.352.2], the second integration in (18) can be calculated as:

$$\begin{aligned} &\int_1^\infty \frac{\exp\left(-\pi \lambda_e (\beta - 1) L^2\right)}{\beta + \frac{\lambda_e}{\lambda_a}} d\beta \\ &= -\exp\left(\pi(\lambda_e + \lambda_a)L^2\right) \text{Ei}\left(-\pi(\lambda_e + \lambda_a)L^2\right). \end{aligned} \quad (20)$$

After plugging (19) and (20) into (18), (17) is obtained. ■

468 *Corollary 3:* When the legitimate user is served by the  
469 nearest AP in its vicinity, the ergodic secrecy rate at the  
470 legitimate user is upper bounded by:

$$471 \quad R_s^{\text{UB}} = \frac{m+3}{\ln(4)} \left( -\exp\left(\pi \lambda_e L^2\right) \text{Ei}\left(-\pi \lambda_e L^2\right) \right). \quad (21)$$

472 *Proof:* The upper bound on the secrecy rate can be  
473 obtained from  $R_s^{\text{UB}} = \lim_{\lambda_a \rightarrow \infty} \mathbb{E}[R_s]$ . Based on the equality

$$474 \quad \lim_{\lambda_a \rightarrow \infty} \exp\left(\pi(\lambda_e + \lambda_a)L^2\right) \text{Ei}\left(-\pi(\lambda_e + \lambda_a)L^2\right) = 0, \quad (22)$$

475 we obtain (21). ■

476 Theorem 2 and Corollary 3 indicate that increasing the density  
477 of VLC APs can help enhance the ergodic secrecy rate of  
478 a typical legitimate user. However, when the density of APs  
479 exceeds a certain level, installing more APs can not enhance  
480 the ergodic secrecy rate any further. While satisfying the  
481 illumination requirement, using LEDs with a smaller semi-  
482 angle can increase the ergodic secrecy rate of a typical user.  
483 Specifically, it can be seen from (17) and (21) that a linear  
484 relationship exists between the ergodic secrecy rate and the  
485 Lambertian order  $m$ . Given the choice of LEDs, the maximum  
486 ergodic secrecy rate can not exceed the upper bound given  
487 in (21). To achieve a target ergodic secrecy rate  $\bar{R}_s$ , whose  
488 value is smaller than  $R_s^{\text{UB}}$ , the density of APs needs to  
489 exceed  $\lambda_a^*$ , where  $\lambda_a^*$  is the numerical solution for  $\lambda_a$  to equa-  
490 tion  $\exp\left(\pi(\lambda_e + \lambda_a)L^2\right) \text{Ei}\left(-\pi(\lambda_e + \lambda_a)L^2\right) = \ln(4)\bar{R}_s /$   
491  $(m+3) + \exp\left(\pi \lambda_e L^2\right) \text{Ei}\left(-\pi \lambda_e L^2\right)$ .

### 492 B. Optimal AP to Serve the Legitimate User

493 Due to the randomness of eavesdroppers, it is not always  
494 optimal to serve the legitimate user with the nearest AP. For  
495 example, if the eavesdropper is close to the nearest AP around  
496 the legitimate user but far away from the second nearest  
497 AP around the legitimate user, selecting the second nearest  
498 AP to serve the legitimate user may yield a higher secrecy  
499 rate. Therefore, with the cooperation among APs, the secrecy  
500 performance at legitimate users can be further enhanced.  
501 However, it should be noted that selecting the optimal AP to  
502 serve legitimate users requires the knowledge of the location  
503 information of all eavesdroppers at the central controller,  
504 which can be achieved with indoor sensing and localization  
505 technologies. Despite the additional implementation and compu-  
506 tation complexity, this optimal scheme yields an enhanced  
507 secrecy rate, which is useful for network designers to quantify  
508 the secrecy performance provided by the nearest AP and  
509 optimal AP and to decide which scheme is more suitable for  
510 practical implementations. When the optimal AP is selected  
511 to serve the legitimate user, the secrecy rate is formulated as:

$$512 \quad R_s = \left[ \max_{x \in \Phi_a} \left\{ \frac{1}{2} \log_2 \left( \frac{P_{\text{rx}}^2(x, o)}{P_{\text{rx}}^2(x, e^*(x))} \right) \right\} \right]^+. \quad (23)$$

513 Due to the intractability of the secrecy rate expression given  
514 in (23), the distribution function of  $R_s$  is hard to obtain. In the  
515 following, we provide two analytical bounds on the CDF of the  
516 secrecy rate.

517 *Corollary 4:* With the cooperation among VLC APs,  
518 the CDF of the secrecy rate at the typical legitimate user is  
519 lower bounded by:

$$520 \quad F_{R_s}(v) \geq \exp\left(-\frac{\lambda_a}{\lambda_e} 4^{-\frac{v}{m+3}} \exp\left(-\pi \lambda_e \left(4^{\frac{v}{m+3}} - 1\right) L^2\right)\right), \quad (24)$$

521 and is upper bounded by:

$$522 \quad F_{R_s}(v) \leq 1 - \frac{1}{1 + \frac{\lambda_e}{\lambda_a} 4^{\frac{v}{m+3}}} \exp\left(-\pi \lambda_e \left(4^{\frac{v}{m+3}} - 1\right) L^2\right). \quad (25)$$

523 *Proof:* With the cooperation of VLC APs, the CDF of the  
524 secrecy rate can be calculated with the help of the probability  
525 generating functional (PGFL) of the PPP [23]:

$$526 \quad \begin{aligned} 527 \quad F_{R_s}(v) &= \mathbb{P} \left[ \max_{x \in \Phi_a} \left\{ \frac{1}{2} \log_2 \left( \frac{P_{\text{rx}}^2(x, o)}{P_{\text{rx}}^2(x, e^*(x))} \right) \right\} \leq v \right] \\ 528 &= \mathbb{P} \left[ \frac{1}{2} \log_2 \left( \frac{P_{\text{rx}}^2(x, o)}{P_{\text{rx}}^2(x, e^*(x))} \right) \leq v, \forall x \in \Phi_a \right] \\ 529 &= \mathbb{E}_{\Phi_e} \left[ \mathbb{E}_{\Phi_a} \left[ \prod_{x \in \Phi_a} \mathbf{1} \left( \|e - x\| \leq \sqrt{\beta L^2 + (\beta - 1)L^2} \right) \right] \right] \\ 530 &= \mathbb{E}_{\Phi_e} \left[ \exp \left[ -\lambda_a \int_{\mathbb{R}^2} \mathbf{1} \left[ \|e - x\| > \sqrt{\beta L^2 + (\beta - 1)L^2} \mid x \right] dx \right] \right], \end{aligned} \quad (26)$$

531 where  $\mathbf{1}(\mathcal{A}) = 1$  with event  $\mathcal{A}$  being true, and zero otherwise.  
532 Based on Jensen's inequality, the lower bound can be calcu-  
533 lated as:

$$534 \quad F_{R_s}(v) \geq \exp \left[ -2\pi \lambda_a \int_0^\infty \mathbb{P} \left[ \|e - x\| > \sqrt{\beta x^2 + (\beta - 1)L^2} \mid x \right] \right. \\ 535 \quad \left. \times x dx \right]. \quad (27)$$

536 After calculating the integration part in (27), the lower bound  
537 result in Corollary 4 is obtained. The upper bound can be  
538 obtained straightforwardly from the following inequality:

$$539 \quad \left[ \max_{x \in \Phi_a} \left\{ \log_2 \left( \frac{P_{\text{rx}}^2(x, o)}{P_{\text{rx}}^2(x, e^*(x))} \right) \right\} \right]^+ \geq \left[ \log_2 \left( \frac{P_{\text{rx}}^2(x_0, o)}{P_{\text{rx}}^2(x_0, e^*(x_0))} \right) \right]^+. \quad (28)$$

540 In other words, choosing the nearest AP to serve the legitimate  
541 user is sub-optimal, which gives an upper bound on the CDF  
542 of the secrecy capacity. Therefore, the upper bound expression  
543 shown in (25) can be obtained directly from Theorem 1. ■

544 Based on the upper bound on the CDF of the secrecy rate,  
545 a lower bound on the ergodic secrecy rate can be obtained,  
546 as given in (17). An upper bound on the ergodic secrecy  
547 rate can be obtained by integrating the complement of the  
548 CDF of  $R_s$ :

$$549 \quad \begin{aligned} 550 \quad \mathbb{E}[R_s] &= \int_0^\infty (1 - F_{R_s}(v)) dv \\ 551 &\leq \frac{m+3}{\ln(4)} \int_1^\infty \left( 1 - \exp \left( -\frac{\lambda_a}{\lambda_e \beta} \exp \left( -\pi \lambda_e (\beta - 1) L^2 \right) \right) \right) \frac{1}{\beta} d\beta. \end{aligned} \quad (29)$$

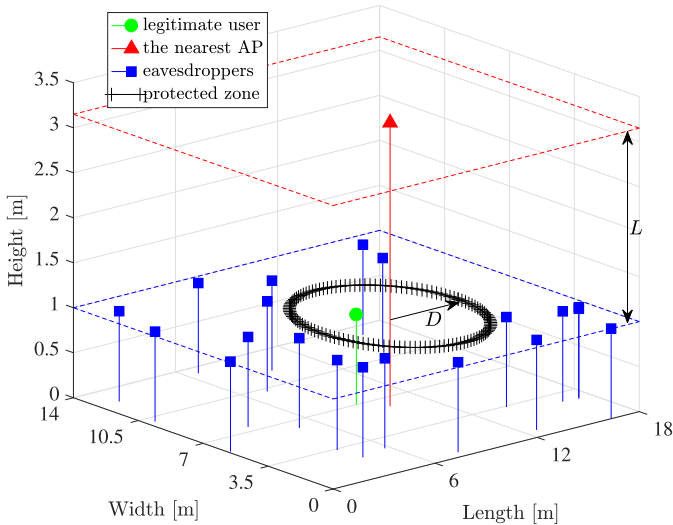


Fig. 2. Random network model with a secrecy protected zone. In this model, each VLC AP has a disk-shaped protected zone, which is centered around the AP and has a radius of  $D$  on the user plane. For simplicity, only the protected zone around the nearest AP is drawn.

Because of the nested exponential function in (29), a closed-form expression is not available. However, (29) can be efficiently calculated using numerical methods.

#### IV. ENHANCING SECURITY RATE IN VLC NETWORKS WITH A PROTECTED ZONE

In order to further enhance the secrecy performance of legitimate users in VLC networks, a strategy named the “protected zone” [34] can be implemented. As depicted in Fig. 2, a protected zone is an eavesdropper-free area (on the user plane), which allows only legitimate users to enter. If any eavesdropper enters the protected zone, such behavior will be made aware to the AP, and the AP will notify the legitimate user and temporarily stop the communication. A practical implementation of the protected zone in VLC networks can be achieved with motion sensors that are already built in modern energy-efficient lighting devices. We acknowledge that there might be means to break the suggested enforcement of the protected zone. However, a deeper investigation of this aspect is outside the scope of this work. A secrecy protected zone can be completely described by its center, i.e., its associated AP, and a security radius  $D$ . The security radius is defined as the smallest horizontal distance between the AP and any eavesdroppers that are undetectable.

*Lemma 1:* Given that the horizontal distance between the nearest AP to the legitimate user is  $x_0$ , the PDF of the horizontal distance between this AP and the nearest eavesdropper, that is outside the protected zone, is:

$$f_{\|e^*(x_0)-x_0\|}(\alpha) = 2\pi\lambda_e\alpha \exp\left(-\pi\lambda_e(\alpha^2 - D^2)\right), \quad (30)$$

for  $\alpha \geq D$ , and zero otherwise.

*Proof:* (30) can be obtained using the void probability of PPP [32]. ■

With Lemma 1, we are ready to obtain the CDF of the secrecy rate enhanced by the protected zone.

*Corollary 5:* When the legitimate user is served by the nearest AP in its vicinity, which has a protected zone with radius  $D$ , the CDF of the enhanced secrecy rate is given by:

$$F_{R_s}(v) = 1 - \frac{\exp\left(-\pi\lambda_e\left(\left(4^{\frac{v}{m+3}} - 1\right)L^2 - D^2\right)\right)}{1 + \frac{\lambda_e}{\lambda_a}4^{\frac{v}{m+3}}}, \quad (31)$$

for  $v \geq \frac{m+3}{2} \log_2(D^2/L^2 + 1)$ , and

$$F_{R_s}(v) = \frac{\exp\left(-\pi\lambda_a\left(D^2 - \left(4^{\frac{v}{m+3}} - 1\right)L^2\right)4^{-\frac{v}{m+3}}\right)}{1 + \frac{\lambda_a}{\lambda_e}4^{-\frac{v}{m+3}}}, \quad (32)$$

for  $0 \leq v < \frac{m+3}{2} \log_2(D^2/L^2 + 1)$ .

*Proof:* Since the protected zone has a radius  $D$ , the minimum distance between the nearest eavesdropper and the AP is  $D$ . Therefore,

$$e^*(x_0) = \arg \min_{e \in \Phi_e, e \notin \mathcal{B}(x_0, D)} \|e - x_0\|, \quad (33)$$

where  $\mathcal{B}(x_0, D)$  denotes the disk-shaped area centered at  $x_0$  with radius  $D$ . Due to the exclusive region in (33), the derivation of the CDF of the enhanced secrecy rate needs to be separated into two scenarios. First, when  $\sqrt{(\beta-1)L^2} \geq D$ , i.e.,  $v \geq \frac{m+3}{2} \log_2(D^2/L^2 + 1)$ , the CDF of the enhanced secrecy rate can be calculated as:

$$F_{R_s}(v) = \int_0^\infty \left(1 - \exp\left(-\pi\lambda_e\left(\beta x_0^2 + (\beta-1)L^2 - D^2\right)\right)\right) \times 2\pi\lambda_a x_0 \exp\left(-\pi\lambda_a x_0^2\right) dx_0, \quad (34)$$

which gives the result in (31). Second, when  $\sqrt{(\beta-1)L^2} < D$ , i.e.,  $0 \leq v < \frac{m+3}{2} \log_2(D^2/L^2 + 1)$ , the CDF of the enhanced secrecy rate can be calculated as:

$$F_{R_s}(v) = \int_{\sqrt{\frac{D^2 - (\beta-1)L^2}{\beta}}}^\infty 2\pi\lambda_a x_0 \exp\left(-\pi\lambda_a x_0^2\right) \times \left(1 - \exp\left(-\pi\lambda_e\left(\beta x_0^2 + (\beta-1)L^2 - D^2\right)\right)\right) dx_0 + \int_0^{\sqrt{\frac{D^2 - (\beta-1)L^2}{\beta}}} 2\pi\lambda_a x_0 \exp\left(-\pi\lambda_a x_0^2\right) \times \mathbb{P}\left[e^*(x_0) \in \mathcal{B}(x_0, D)\right] dx_0, \quad (35)$$

in which the critical point  $x_0 = \sqrt{(D^2 - (\beta-1)L^2)/\beta}$  is found by solving  $\sqrt{\beta x_0^2 + (\beta-1)L^2} = D$ . Since  $e^*(x_0) \notin \mathcal{B}(x_0, D)$ ,  $\mathbb{P}\left[e^*(x_0) \in \mathcal{B}(x_0, D)\right] = 0$ , and the second integration in (35) reduces to zero. After calculating the first integration in (35), we obtain (32). To this end, the proof is completed. ■

It can be seen from Corollary 5 that the radius of the protected zone has a strong impact on the CDF of the secrecy rate and on the secrecy outage probability. On the one hand, if the radius of the protected zone is small enough so that the target secrecy rate satisfies  $\bar{R}_s \geq \frac{m+3}{2} \log_2(D^2/L^2 + 1)$ , given a fixed density of eavesdroppers, the secrecy outage probability is lower bounded by:

$$P_{so}^{LB} = 1 - \exp\left(-\pi\lambda_e\left(\left(4^{\frac{\bar{R}_s}{m+3}} - 1\right)L^2 - D^2\right)\right), \quad (36)$$



629 which is obtained when the density of the APs goes to  
 630 infinity. On the other hand, if the radius of the protected  
 631 zone is large enough so that the target secrecy rate satisfies  
 632  $\bar{R}_s < \frac{m+3}{2} \log_2(D^2/L^2 + 1)$ , increasing the density of VLC  
 633 APs can efficiently reduce the secrecy outage probability, and  
 634 the worst-case scenario of the secrecy outage probability is  
 635 upper bounded by:

$$636 p_{\text{so}}^{\text{UB}} = \exp\left(-\pi \lambda_a \left(D^2 - \left(4^{\frac{\bar{R}_s}{m+3}} - 1\right) L^2\right) 4^{-\frac{\bar{R}_s}{m+3}}\right), \quad (37)$$

637 which is obtained by letting  $\lambda_e$  approach infinity.

638 Corollary 5 provides an essential guideline to network  
 639 designers so that they can design a suitable protected zone  
 640 around each VLC AP in order to provide legitimate users  
 641 with guaranteed secrecy service. Specifically, for legitimate  
 642 users to achieve a target secrecy rate  $\bar{R}_s$  with a target  
 643 secrecy outage probability  $\bar{p}_{\text{so}}$ , network designers can set up  
 644 the protected zone with radius no smaller than  $D^*$ , where  
 645  $D^* = ((4^{\bar{R}_s/(m+3)} - 1)L^2 + (\ln(1 - \bar{p}_{\text{so}}) + \ln(1 + 4^{\bar{R}_s/(m+3)} \lambda_e/\lambda_a)) / \pi \lambda_e)^{1/2}$  for  $\bar{p}_{\text{so}} \geq 1 - (1 + 4^{\bar{R}_s/(m+3)} \lambda_e/\lambda_a)^{-1}$ ,  
 646 and  $D^* = ((4^{\bar{R}_s/(m+3)} - 1)L^2 - (\ln \bar{p}_{\text{so}} + \ln(1 + 4^{-\bar{R}_s/(m+3)} \lambda_a/\lambda_e)) / \pi \lambda_a)^{1/2}$  for  $\bar{p}_{\text{so}} < 1 - (1 + 4^{\bar{R}_s/(m+3)} \lambda_e/\lambda_a)^{-1}$ . Also, it is evident that a more stringent  
 647 secrecy requirement with a larger  $\bar{R}_s$  and/or a smaller  $\bar{p}_{\text{so}}$   
 648 requires the implementation of a larger secrecy protected zone.

649 *Theorem 3:* When the legitimate user is served by the  
 650 nearest AP in its vicinity, which has a protected zone with  
 651 radius  $D$ , the enhanced ergodic secrecy rate at the typical  
 652 legitimate user is:

$$653 \mathbb{E}[R_s] \\
 654 = \frac{m+3}{\ln(4)} \left[ -\exp(\pi \lambda_e (L^2 + D^2)) \text{Ei}(-\pi \lambda_e (L^2 + D^2)) \right. \\
 655 \left. + \ln\left(\frac{D^2}{L^2} + 1\right) \right] + \frac{m+3}{\ln(4)} \exp(\pi \lambda_a L^2) \left[ \text{Ei}(-\pi \lambda_a L^2) \right. \\
 656 \left. + \exp(\pi \lambda_e (L^2 + D^2)) \text{Ei}(-\pi (\lambda_a + \lambda_e) (L^2 + D^2)) \right. \\
 657 \left. - \text{Ei}(-\pi \lambda_a (L^2 + D^2)) \right]. \quad (38)$$

658 *Proof:* Based on Corollary 5, the enhanced ergodic rate  
 659 can be calculated by integrating the complement of the CDF.  
 660 Since the CDF has different expressions at different regions,  
 661 the integration should be separated into two parts:

$$662 \mathbb{E}[R_s] \\
 663 = \frac{m+3}{\ln(4)} \int_1^{\frac{D^2}{L^2}+1} \left( 1 - \frac{\exp\left(\frac{-\pi \lambda_a (D^2 - (\beta-1)L^2)}{\beta}\right)}{1 + \frac{\lambda_a}{\lambda_e} \frac{1}{\beta}} \right) \frac{1}{\beta} d\beta \\
 664 + \frac{m+3}{\ln(4)} \int_{\frac{D^2}{L^2}+1}^{\infty} \frac{\exp(-\pi \lambda_e ((\beta-1)L^2 - D^2))}{\beta + \frac{\lambda_a}{\lambda_e} \beta^2} d\beta, \quad (39)$$

665 where for simplicity the variable of integration has been  
 666 changed from  $v$  to  $\beta$ . The first integration in (39) can be

simplified to:

$$670 \int_1^{\frac{D^2}{L^2}+1} \left( 1 - \frac{\exp\left(\frac{-\pi \lambda_a (D^2 - (\beta-1)L^2)}{\beta}\right)}{1 + \frac{\lambda_a}{\lambda_e} \frac{1}{\beta}} \right) \frac{1}{\beta} d\beta \\
 671 = \ln\left(\frac{D^2}{L^2} + 1\right) + \exp(\pi \lambda_a L^2) \\
 672 \times \int_1^{\frac{D^2}{L^2}+1} \frac{\exp\left(\frac{-\pi \lambda_a (L^2 + D^2)}{\beta}\right)}{\beta + \frac{\lambda_a}{\lambda_e}} d\beta, \quad (40)$$

673 in which the integration part can be obtained as:

$$674 \int_1^{\frac{D^2}{L^2}+1} \frac{\exp\left(\frac{-\pi \lambda_a (L^2 + D^2)}{\beta}\right)}{\beta + \frac{\lambda_a}{\lambda_e}} d\beta \\
 675 = \text{Ei}(-\pi \lambda_a L^2) - \text{Ei}(-\pi \lambda_a (L^2 + D^2)) \\
 676 + \exp(\pi \lambda_e (L^2 + D^2)) \text{Ei}(-\pi (\lambda_a + \lambda_e) (L^2 + D^2)) \\
 677 - \exp(\pi \lambda_e (L^2 + D^2)) \text{Ei}(-\pi \lambda_a L^2 - \pi \lambda_e (L^2 + D^2)). \quad (41)$$

678 Similarly, the second integration in (39) can be simplified to:

$$679 \int_{\frac{D^2}{L^2}+1}^{\infty} \frac{\exp(-\pi \lambda_e ((\beta-1)L^2 - D^2))}{\beta + \frac{\lambda_a}{\lambda_e} \beta^2} d\beta \\
 680 = \exp(\pi \lambda_e (L^2 + D^2)) \left[ \int_{\frac{D^2}{L^2}+1}^{\infty} \frac{\exp(-\pi \lambda_e \beta L^2)}{\beta} d\beta \right. \\
 681 \left. - \int_{\frac{D^2}{L^2}+1}^{\infty} \frac{\exp(-\pi \lambda_e \beta L^2)}{\beta + \frac{\lambda_a}{\lambda_e}} d\beta \right]. \quad (42)$$

682 Applying [33, eq. 3.352.2], the two integrations in (42) can  
 683 be calculated as:

$$684 \int_{\frac{D^2}{L^2}+1}^{\infty} \frac{\exp(-\pi \lambda_e \beta L^2)}{\beta} d\beta = -\text{Ei}(-\pi \lambda_e (L^2 + D^2)), \quad (43)$$

685 and

$$686 \int_{\frac{D^2}{L^2}+1}^{\infty} \frac{\exp(-\pi \lambda_e \beta L^2)}{\beta + \frac{\lambda_a}{\lambda_e}} d\beta \\
 687 = -\exp(\pi \lambda_a L^2) \text{Ei}\left(-\pi \lambda_e L^2 \left(\frac{\lambda_a}{\lambda_e} + \frac{D^2}{L^2} + 1\right)\right). \quad (44)$$

688 Combining (40) – (44) gives the result shown in (38), which  
 689 completes the proof. ■

690 Note that the expression for the ergodic secrecy rate in  
 691 Theorem 3 can be simplified to the one given in Theorem 2  
 692 when  $D = 0$ . Also, it is shown in Theorem 3 that the ergodic  
 693 secrecy rate scales linearly with the Lambertian order  $m$ ,  
 694 regardless of the size of the protected zone. Given the choice  
 695 of LEDs, the density of APs and the density of eavesdroppers,  
 696 a target ergodic secrecy capacity  $\bar{R}_s$  can be achieved through  
 697 the implementation of a protected zone with radius  $D^*$ , where  
 698

TABLE I  
SIMULATION PARAMETERS

Parameter	value
Room dimensions	$18 \times 14 \times 3.5 \text{ m}^3$
Height of VLC APs	3.15 m
Height of mobile users	1 m
Semi-angle of VLC APs, $\Phi_{1/2}$	$30^\circ$
Transmit optical power of VLC APs, $P_{\text{tx}}$	1 W
Receiver detection area, $A$	$1 \text{ cm}^2$
Receiver responsivity, $\eta$	0.4 A/W
Reflective index of the optical concentrator, $n$	1.5
Optical filter gain, $T$	1
Receiver FOV, $\Psi_{\text{fov}}$	$90^\circ$
Receiver noise power, $\sigma_{\text{nb}}^2 = \sigma_{\text{nc}}^2$	-103.98 dBm

700  $D^*$  is the numerical solution for  $D$  by letting (38) equal  $\bar{R}_s$ .  
701 Since the expression in (38) monotonically increases with  
702 respect to  $D$ , the numerical solution for  $D^*$  is unique.

## V. SIMULATION RESULTS AND DISCUSSIONS

### A. Results Based on the PPP Model

705 In this section, we use a MATLAB implementation to  
706 validate the derived results. Simulation results are obtained  
707 by averaging 20,000 realizations of Monte Carlo simulations.  
708 A typical office of size  $18 \times 14 \times 3.5 \text{ m}^3$  is considered,  
709 as illustrated in Figs. 1 and 2. If not otherwise specified,  
710 the network parameters used for the simulation setup are  
711 described in Table I.

712 First, we consider the scenario where the legitimate user is  
713 served by the nearest AP in its vicinity, without the imple-  
714 mentation of the secrecy protected zone. Therefore, malicious  
715 eavesdroppers can be horizontally as close as possible to the  
716 AP that serves the legitimate user. By fixing the density of  
717 eavesdroppers ( $\lambda_e = 0.2$ ), the secrecy outage probability at  
718 the typical legitimate user is evaluated at different values of  
719 the AP density, as shown in Fig. 3. It can be seen that,  
720 when  $\lambda_a$  is small, increasing the density of VLC APs can  
721 efficiently reduce the secrecy outage probability at the legiti-  
722 mate user. However, when  $\lambda_a$  is large, further increasing the  
723 density of VLC APs only slightly reduces the secrecy outage  
724 probability. For example, given that the target secrecy rate is  
725  $\bar{R}_s = 1 \text{ bit/s/Hz}$ , increasing  $\lambda_a$  from 0.1 to 1 can cause the  
726 secrecy outage probability to drop by 0.3. In comparison, when  
727  $\lambda_a$  is increased from 1 to 10, the secrecy outage probability  
728 only drops by 0.1. Also, it is shown that a lower bound on  
729 the secrecy outage probability exists even if the density of  
730 VLC APs approaches infinity. This result is in agreement  
731 with Corollary 2. In Fig. 4, the ergodic secrecy rate is plotted  
732 against the density of APs. It is shown that the ergodic secrecy  
733 rate at the legitimate user drops when the density of eaves-  
734 droppers increases. Given a fixed density of eavesdroppers,  
735 increasing the density of VLC APs can efficiently enhance the  
736 ergodic secrecy rate when  $\lambda_a$  is small. However, the ergodic  
737 secrecy rate of the legitimate user tends to saturate at high  
738 AP densities. As a result, increasing the density of VLC APs  
739 when  $\lambda_a$  is large does not bring a significant incrementation  
740 to the ergodic secrecy rate. Instead, increasing the density of  
741 APs when  $\lambda_a$  is small is more meaningful.

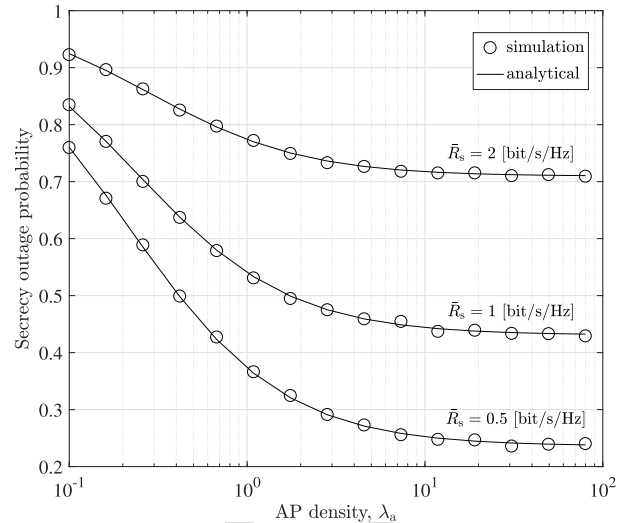


Fig. 3. Secrecy outage probability versus VLC AP density. The legitimate user is served by the nearest AP in its vicinity.  $\lambda_e = 0.2$ .

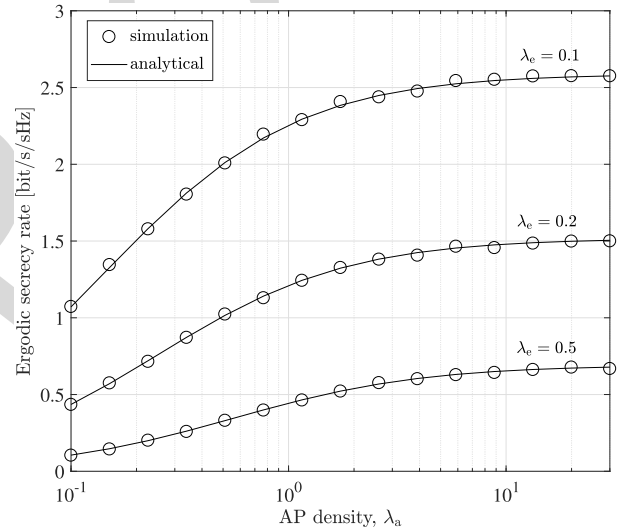


Fig. 4. Ergodic secrecy rate versus VLC AP density. The legitimate user is served by the nearest AP in its vicinity.

742 Second, we consider the scenario where the legitimate user  
743 is served by the optimal AP when APs are cooperated in the  
744 network. For the typical legitimate user, the optimal AP is  
745 not necessarily the nearest one, depending on the locations  
746 of potential eavesdroppers. With the cooperation among VLC  
747 APs, the optimal AP that brings the highest secrecy rate to  
748 the legitimate user is selected. For Monte Carlo simulations,  
749 the optimal AP is found out through the exhaustive search  
750 method. In Fig. 5, the secrecy outage probability is plotted  
751 against different eavesdropper densities, and it can be seen  
752 that the simulation results are well bounded by the derived  
753 analytical results. On the one hand, by assuming that the  
754 optimal AP is the nearest one, we underestimate the secrecy  
755 rate at the legitimate user. As a result, this assumption leads to  
756 an upper bound on the secrecy outage probability. On the other  
757 hand, the lower bound on the secrecy outage probability is

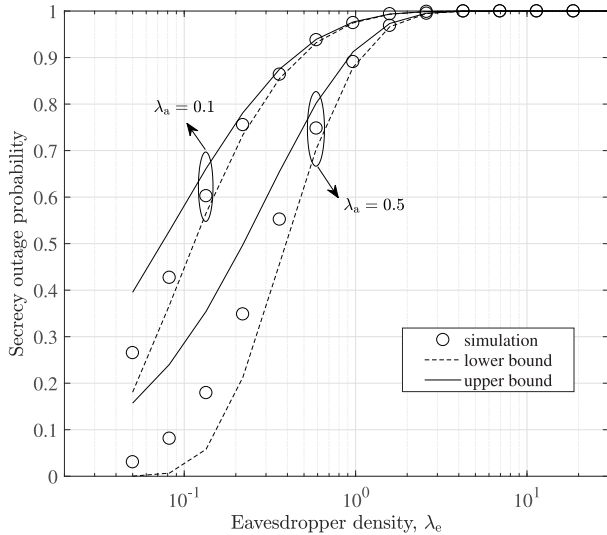


Fig. 5. Secrecy outage probability versus eavesdropper density. The legitimate user is served by the optimal AP.  $\bar{R}_s = 0.5$  bit/s/Hz.

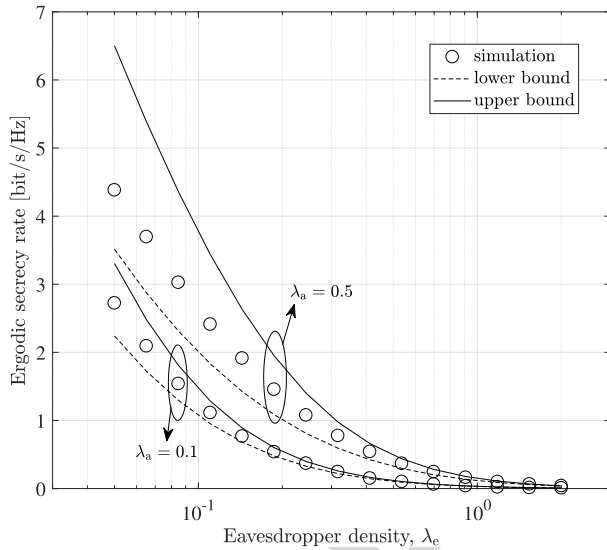


Fig. 6. Ergodic secrecy rate versus eavesdropper density. The legitimate user is served by the optimal AP.

obtained from Jensen's inequality, as described in Corollary 4. Comparing the lower bound with the upper bound, it can be seen that the lower bound is closer to the simulation results. It is also shown in Fig. 5 that both theoretical bounds on the secrecy outage probability are reasonably tight when the eavesdropper density is large. In Fig. 6, the ergodic secrecy rate at the legitimate user is computed for different values of the eavesdropper density. It should be noted that assuming the optimal AP is the nearest one gives the lower bound on the ergodic secrecy rate in Fig. 6, which corresponds to the upper bound on the secrecy outage probability in Fig. 5. Again, both analytical bounds become tighter as the eavesdropper density increases. Based on the results shown in Fig. 5 and Fig. 6, we can conclude that the optimal AP that maximizes the secrecy performance at the legitimate user is not necessarily the nearest one. To investigate deeper, we show in Fig. 7

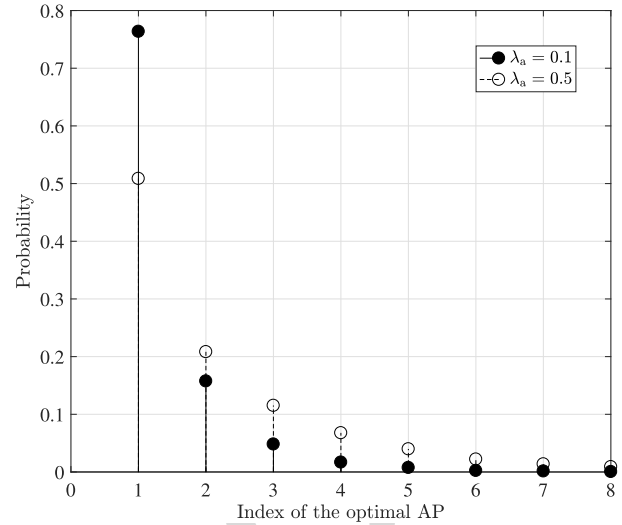


Fig. 7. Probability mass function (PMF) of the index of the optimal AP.  $\lambda_e = 0.2$ .

the probability mass function (PMF) of the index of the optimal AP that maximizes the secrecy rate at the legitimate user. Index  $i$  relates to the  $i$ -th nearest neighboring AP to the legitimate user. For example, index 1 corresponds to the nearest AP, index 2 corresponds to the second nearest AP, and so on. It is shown in Fig. 7 that, compared to other neighboring APs, the nearest AP is most likely the optimal one. However, it is also possible that the optimal AP is the second nearest, third nearest, etc. Fig. 7 also shows that with a smaller value of  $\lambda_a$ , it is more likely that the nearest AP is the optimal one, which therefore explains why the analytical bounds are tighter for smaller values of  $\lambda_a$ , as observed in Fig. 5 and Fig. 6.

Third, we consider the scenario where the legitimate user is served by the nearest AP in its vicinity, with the implementation of a secrecy protected zone. It is assumed that any malicious eavesdroppers that are inside the protected zone can be detected by the AP so that these eavesdroppers do not cause any secrecy information loss at the legitimate user. As a result, the secrecy information loss at the legitimate user is caused by the eavesdroppers that are outside the protected zone only. In Fig. 8, the secrecy outage probability is plotted against the density of VLC APs. It is shown that, for a given target secrecy rate, the secrecy outage probability decreases as the AP density increases. However, when  $\lambda_a$  is large, further increasing the density of VLC APs only slightly reduces the secrecy outage probability. Also, it is shown that there exists a lower bound on the secrecy outage probability when  $\lambda_a$  approaches infinity. After implementing a secrecy protected zone with radius  $D$ , the secrecy outage probability is reduced significantly. More specifically, when  $\lambda_a = 1$ ,  $\lambda_e = 0.2$  and the target secrecy rate is  $\bar{R}_s = 2$  bit/s/Hz, implementing a secrecy protected zone with radius  $D = 1$  m reduces the secrecy outage probability by 0.2. If the secrecy protected zone has a radius of  $D = 2$  m, the secrecy outage probability can be reduced to nearly zero. It is also shown in Fig. 8 that, with a sufficiently large protected area, the secrecy outage probability is no longer bounded at the lower end, i.e., increasing the density of VLC

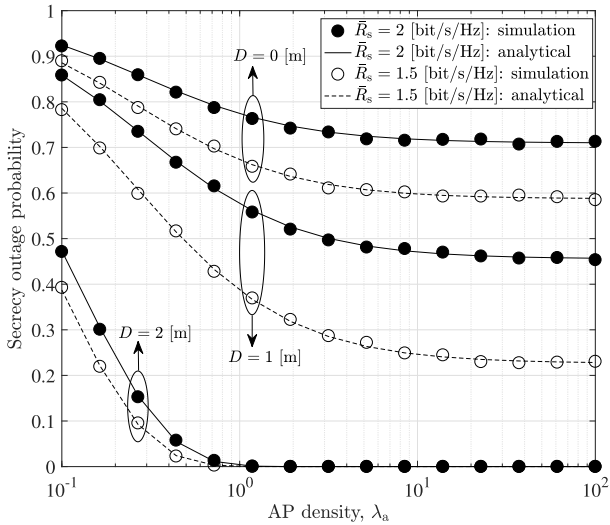


Fig. 8. Secrecy outage probability versus VLC AP density. The legitimate user is served by the nearest AP in its vicinity, and eavesdroppers are outside the protected zone with radius  $D$ .  $\lambda_e = 0.2$ .

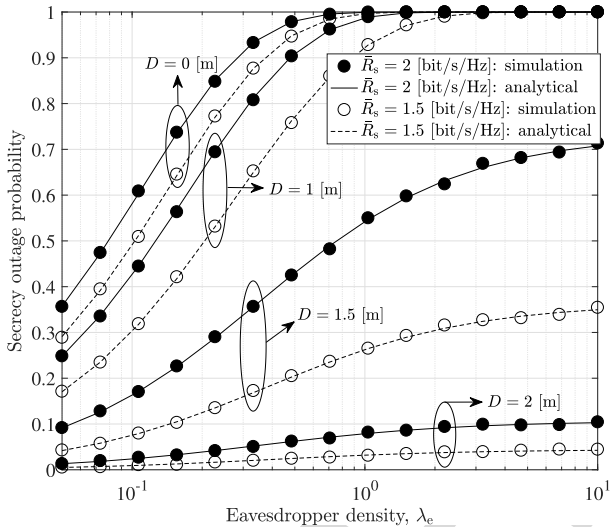


Fig. 9. Secrecy outage probability versus eavesdropper density. The legitimate user is served by the nearest AP in its vicinity, and eavesdroppers are outside the protected zone with radius  $D$ .  $\lambda_a = 0.5$ .

811 APs can efficiently reduce the secrecy outage probability to  
 812 zero. In Fig. 9, we fix  $\lambda_a = 0.5$  and evaluate the impact of  
 813 the eavesdropper density on the secrecy outage probability.  
 814 It can be seen that, without the protected zone, the secrecy  
 815 outage probability can be as large as one if the eavesdropper  
 816 density is sufficiently high. However, with the implementa-  
 817 tion of a protected zone, the worst-case scenario of the secrecy  
 818 outage probability can be limited below a certain level. For  
 819 example, when the target secrecy rate is  $\bar{R}_s = 2$  bit/s/Hz and  
 820 the protected zone has a radius of  $D = 2$  m, the worst-case  
 821 secrecy outage probability at the legitimate user does not  
 822 exceed 0.12, regardless of the eavesdropper density. To fur-  
 823 ther investigate the impact of the protected zone, we show  
 824 in Fig. 10 the ergodic secrecy rate against the radius of the  
 825 protected zone while fixing the eavesdropper density to  
 826  $\lambda_e = 0.2$ . The slope of the curve shows that a very small  
 827 protected area brings only marginal improvement on the

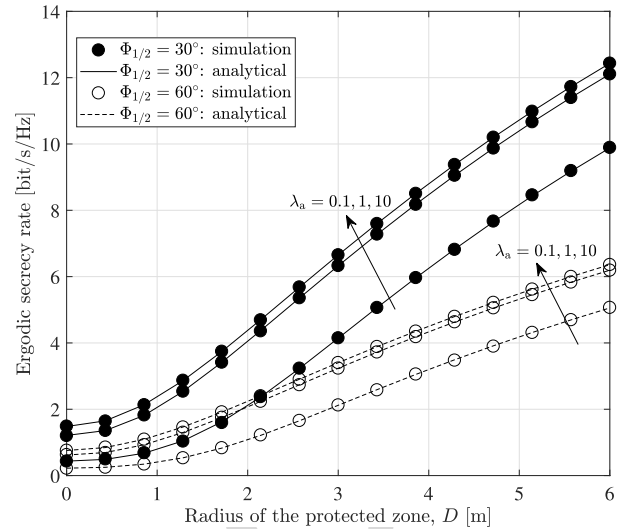


Fig. 10. Ergodic secrecy rate versus the radius of the protected zone. The legitimate user is served by the nearest AP in its vicinity.  $\lambda_e = 0.2$ .

828 secrecy performance. However, by increasing the size of  
 829 the protected zone further, the secrecy performance at the  
 830 legitimate user can be enhanced significantly. Specifically,  
 831 when  $\lambda_a = 1$  and  $\Phi_{1/2} = 30^\circ$ , increasing the radius of the  
 832 protected zone from 0 to 1 m increases the ergodic secrecy  
 833 rate by 0.6 bit/s/Hz. In contrast, increasing the radius of  
 834 the protected zone from 1 to 2 m can increase the ergodic  
 835 secrecy rate by 1.9 bit/s/Hz. In Fig. 10, it is also shown that  
 836 using more directional LEDs, i.e., LEDs with a smaller semi-  
 837 angle, enhances the secrecy performance at the legitimate user.  
 838 However, the actual choice of LEDs should also take practical  
 839 illumination requirements into consideration.

840 **B. PPP Model vs. Grid Model**

841 In the following, we compare the secrecy performance  
 842 between the stochastic PPP model and the deterministic grid  
 843 model. For the grid model, it implicitly assumes that the  
 844 number of APs, as well as their locations in the network, are  
 845 fixed and known. As shown in Fig. 11 and Fig. 12, we use a  
 846 hexagonal-shaped grid to model the locations of APs within  
 847 the same indoor space. A total number of 31 APs (represented  
 848 by red triangles) are considered, and without loss of generality  
 849 the secrecy performance is studied by focusing on the central  
 850 hexagonal cell. A legitimate user (represented by the green  
 851 circle) is randomly distributed within the central cell and is  
 852 served by the central AP. The eavesdroppers (represented by  
 853 blue squares) are assumed to follow a Poisson distribution  
 854 with intensity  $\lambda_e$ . To allow for a fair comparison between  
 855 the PPP model and the grid model, the density of APs in  
 856 the PPP model is set to 0.12 so that the expected number  
 857 of APs in the PPP model equals the total number of APs  
 858 in the grid model. It can be seen from Fig. 11 that the  
 859 PPP model and the grid model yield similar results for the  
 860 secrecy outage probability. Both curves have similar shapes  
 861 and trends, especially for higher target secrecy rates and  
 862 with larger eavesdropper densities. In general, the grid model

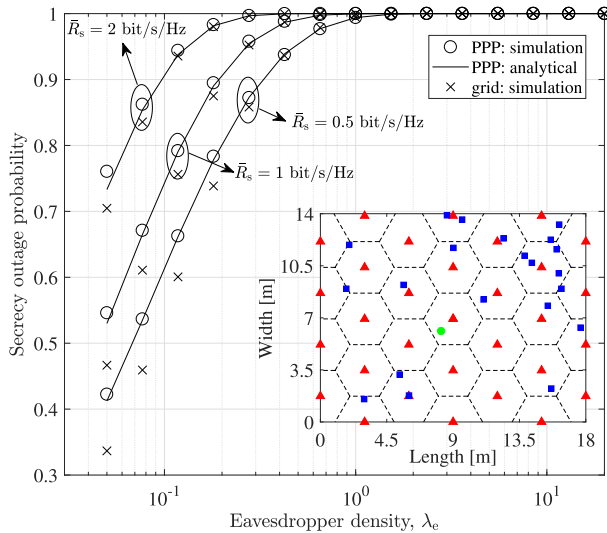


Fig. 11. Secrecy outage probability comparison between the PPP model and the grid model.  $\lambda_a = 0.12$ .

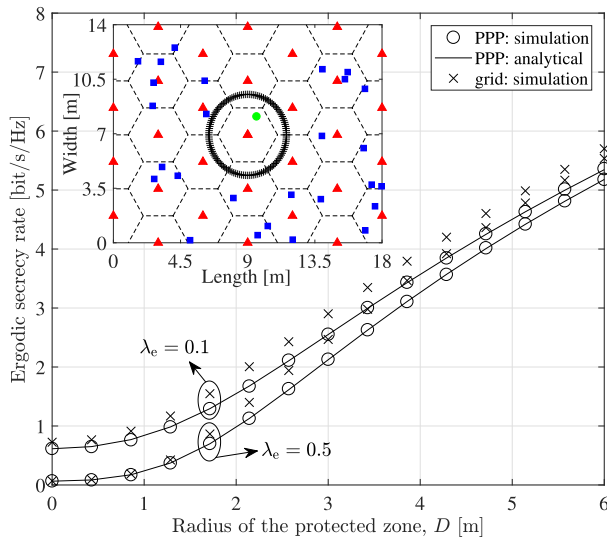


Fig. 12. Ergodic secrecy rate comparison between the PPP model and the grid model.  $\lambda_a = 0.12$ .

provides slightly superior coverage performance than the PPP model because of its more regularized cell shapes. With the implementation of a secrecy protected zone, we compare in Fig. 12 the achieved ergodic secrecy rate between the PPP model and the grid model. The configuration of the grid model in Fig. 12 is the same as that in Fig. 11, except that the eavesdroppers are prohibited in the circular protected zone centered around the central AP. Results show that both models yield close ergodic secrecy rates, especially for networks with more populated eavesdroppers.

## VI. CONCLUSION

In this work, we studied the performance of physical-layer secrecy in a three-dimensional multiuser VLC network. With the use of mathematical tools from stochastic geometry, analytical expressions for the secrecy outage probability, the ergodic secrecy rate, as well as their lower and upper bounds, are

derived in tractable forms and verified through Monte Carlo simulations. Impacts of AP cooperation and the implementation of a secrecy protected zone on the secrecy performance have also been investigated. Results show that cooperating neighboring APs can enhance the secrecy performance of VLC networks, but only to a limited extent. We also show that building a secrecy protected zone around the AP significantly improves the network secrecy performance.

Justifying the application of the PPP model to the performance analysis of VLC networks is an important research direction. Also, improved stochastic models may be developed in the future to more accurately capture the spatial distribution of APs in a real network deployment.

## REFERENCES

- [1] T. Komine and M. Nakagawa, "Fundamental analysis for visible-light communication system using LED lights," *IEEE Trans. Consum. Electron.*, vol. 50, no. 1, pp. 100–107, Feb. 2004.
- [2] S. Dimitrov and H. Haas, *Principles of LED Light Communications: Towards Networked Li-Fi*. Cambridge, U.K.: Cambridge Univ. Press, 2015.
- [3] H. Haas, L. Yin, Y. Wang, and C. Chen, "What is Li-Fi?" *J. Lightw. Technol.*, vol. 34, no. 6, pp. 1533–1544, Mar. 15, 2016.
- [4] *IEEE Standard for Local and Metropolitan Area Networks—Part 15.7: Short-Range Wireless Optical Communication Using Visible Light*, IEEE Computer Society, IEEE Standard 802.15.7-2011, 2011.
- [5] X. Li, F. Jin, R. Zhang, J. Wang, Z. Xu, and L. Hanzo, "Users first: User-centric cluster formation for interference-mitigation in visible-light networks," *IEEE Trans. Wireless Commun.*, vol. 15, no. 1, pp. 39–53, Jan. 2016.
- [6] H. Ma, L. Lampe, and S. Hranilovic, "Coordinated broadcasting for multiuser indoor visible light communication systems," *IEEE Trans. Commun.*, vol. 63, no. 9, pp. 3313–3324, Sep. 2015.
- [7] L. Yin, W. O. Popoola, X. Wu, and H. Haas, "Performance evaluation of non-orthogonal multiple access in visible light communication," *IEEE Trans. Commun.*, vol. 64, no. 12, pp. 5162–5175, Dec. 2016.
- [8] A. D. Wyner, "The wire-tap channel," *Bell Syst. Tech. J.*, vol. 54, no. 8, pp. 1355–1387, 1975.
- [9] I. Csiszár and J. Körner, "Broadcast channels with confidential messages," *IEEE Trans. Inf. Theory*, vol. IT-24, no. 3, pp. 339–348, May 1978.
- [10] M. Haenggi, "The secrecy graph and some of its properties," in *Proc. IEEE Int. Symp. Inf. Theory*, Toronto, ON, Canada, Jul. 2008, pp. 539–543.
- [11] P. C. Pinto, J. Barros, and M. Z. Win, "Secure communication in stochastic wireless networks—Part I: Connectivity," *IEEE Trans. Inf. Forensics Security*, vol. 7, no. 1, pp. 125–138, Feb. 2012.
- [12] P. C. Pinto, J. Barros, and M. Z. Win, "Secure communication in stochastic wireless networks—Part II: Maximum rate and collusion," *IEEE Trans. Inf. Forensics Security*, vol. 7, no. 1, pp. 139–147, Feb. 2012.
- [13] O. O. Koyluoglu, C. E. Koksal, and H. El Gamal, "On secrecy capacity scaling in wireless networks," *IEEE Trans. Inf. Theory*, vol. 58, no. 5, pp. 3000–3015, May 2012.
- [14] X. Zhou, R. K. Ganti, J. G. Andrews, and A. Hjørungnes, "On the throughput cost of physical layer security in decentralized wireless networks," *IEEE Trans. Wireless Commun.*, vol. 10, no. 8, pp. 2764–2775, Aug. 2011.
- [15] H. Wang, X. Zhou, and M. C. Reed, "Physical layer security in cellular networks: A stochastic geometry approach," *IEEE Trans. Wireless Commun.*, vol. 12, no. 6, pp. 2776–2787, Jun. 2013.
- [16] A. Lapidath, S. M. Moser, and M. A. Wigger, "On the capacity of free-space optical intensity channels," *IEEE Trans. Inf. Theory*, vol. 55, no. 10, pp. 4449–4461, Oct. 2009.
- [17] J.-B. Wang, Q.-S. Hu, J. Wang, M. Chen, and J.-Y. Wang, "Tight bounds on channel capacity for dimmable visible light communications," *J. Lightw. Technol.*, vol. 31, no. 23, pp. 3771–3779, Dec. 1, 2013.
- [18] A. Chaaban, J. M. Morvan, and M. S. Alouini, "Free-space optical communications: Capacity bounds, approximations, and a new sphere-packing perspective," *IEEE Trans. Commun.*, vol. 64, no. 3, pp. 1176–1191, Mar. 2016.

- 948 [19] S. Dimitrov and H. Haas, "Information rate of OFDM-based optical  
949 wireless communication systems with nonlinear distortion," *J. Lightw.  
950 Technol.*, vol. 31, no. 6, pp. 918–929, Mar. 15, 2013.
- 951 [20] A. Mostafa and L. Lampe, "Physical-layer security for MISO visible  
952 light communication channels," *IEEE J. Sel. Areas Commun.*, vol. 33,  
953 no. 9, pp. 1806–1818, Sep. 2015.
- 954 [21] A. Mostafa and L. Lampe, "Optimal and robust beamforming for  
955 secure transmission in MISO visible-light communication links,"  
956 *IEEE Trans. Signal Process.*, vol. 64, no. 24, pp. 6501–6516,  
957 Dec. 2016.
- 958 [22] G. Pan, J. Ye, and Z. Ding, "On secure VLC systems with spatially  
959 random terminals," *IEEE Commun. Lett.*, vol. 21, no. 3, pp. 492–495,  
960 Mar. 2016.
- 961 [23] D. Stoyan, W. Kendall, and J. Mecke, *Stochastic Geometry and its  
962 Applications*, 2nd ed. Hoboken, NJ, USA: Wiley, 1996.
- 963 [24] L. Zeng *et al.*, "High data rate multiple input multiple output  
964 (MIMO) optical wireless communications using white LED light-  
965 ing," *IEEE J. Sel. Areas Commun.*, vol. 27, no. 9, pp. 1654–1662,  
966 Dec. 2009.
- 967 [25] J. Grubor, S. Randel, K. D. Langer, and J. W. Walewski, "Broadband  
968 information broadcasting using LED-based interior lighting," *J. Lightw.  
969 Technol.*, vol. 26, no. 24, pp. 3883–3892, Dec. 15, 2008.
- 970 [26] J. M. Kahn and J. R. Barry, "Wireless infrared communications," *Proc.  
971 IEEE*, vol. 85, no. 2, pp. 265–298, Feb. 1997.
- 972 [27] L. Hanzo, H. Haas, S. Imre, D. O'Brien, M. Rupp, and L. Gyongyosi,  
973 "Wireless myths, realities, and futures: From 3G/4G to optical and  
974 quantum wireless," *Proc. IEEE*, vol. 100, pp. 1853–1888, May 2012.
- 975 [28] C. Chen, S. Videv, D. Tsonev, and H. Haas, "Fractional frequency reuse  
976 in DCO-OFDM-based optical attocell networks," *J. Lightw. Technol.*,  
977 vol. 33, no. 19, pp. 3986–4000, Oct. 1, 2015.
- 978 [29] S. Leung-Yan-Cheong and M. E. Hellman, "The Gaussian wire-tap  
979 channel," *IEEE Trans. Inf. Theory*, vol. IT-24, no. 4, pp. 451–456,  
980 Jul. 1978.
- 981 [30] O. Ozel, E. Ekrem, and S. Ulukus, "Gaussian wiretap channel with  
982 an amplitude constraint," in *Proc. IEEE Inf. Theory Workshop (ITW)*,  
983 Sep. 2012, pp. 139–143.
- 984 [31] M. Haenggi, "On distances in uniformly random networks," *IEEE Trans.  
985 Inf. Theory*, vol. 51, no. 10, pp. 3584–3586, Oct. 2005.
- 986 [32] S. Srinivasa and M. Haenggi, "Distance distributions in finite uniformly  
987 random networks: Theory and applications," *IEEE Trans. Veh. Technol.*,  
988 vol. 59, no. 2, pp. 940–949, Feb. 2010.
- 989 [33] I. S. Gradshteyn and I. M. Ryzhik, *Tables of Integrals, Series, and  
990 Products*, 7th ed. San Diego, CA, USA: Academic, 2007.
- 991 [34] N. Romero-Zurita, D. McLernon, M. Ghogho, and A. Swami, "PHY  
992 layer security based on protected zone and artificial noise," *IEEE Signal  
993 Process. Lett.*, vol. 20, no. 5, pp. 487–490, May 2013.



**Liang Yin** received the B.Eng. degree (Hons.) in 994  
electronics and electrical engineering from the 995  
University of Edinburgh, Edinburgh, U.K., in 2014, 996  
where he is currently pursuing the Ph.D. degree in 997  
electrical engineering. His research interests are in 998  
visible light communication and positioning, multi- 999  
user networking, and wireless network performance 1000  
analysis. He received the Class Medal Award and 1001  
IET Prize Award from the University of Edinburgh. 1002



**Harald Haas** (S'98–AM'00–M'03–SM'17) 1003  
received the Ph.D. degree from the University of 1004  
Edinburgh in 2001. He currently holds the Chair 1005  
of mobile communications with the University of 1006  
Edinburgh, and is the Initiator, Co-Founder, and 1007  
the Chief Scientific Officer of pureLiFi Ltd and 1008  
the Director of the LiFi Research and Development 1009  
Center, University of Edinburgh. He has authored 1010  
400 conference and journal papers including a 1011  
paper in Science and co-authored a book entitled 1012  
*Principles of LED Light Communications Towards* 1013

*Networked Li-Fi* (Cambridge University Press, 2015). His main research 1014  
interests are in optical wireless communications, hybrid optical wireless 1015  
and RF communications, spatial modulation, and interference coordination 1016  
in wireless networks. He first introduced and coined spatial modulation 1017  
and LiFi. LiFi was listed among the 50 best inventions in TIME Magazine 1018  
2011. He was an invited speaker with TED Global 2011, and his talk 1019  
on Wireless Data from Every Light Bulb has been watched online over 1020  
2.4 million times. He gave a second TED Global lecture in 2015 on the 1021  
use of solar cells as LiFi data detectors and energy harvesters. This has 1022  
been viewed online over 1.8 million times. He was elected as a Fellow 1023  
of the Royal Society of Edinburgh in 2017. In 2012 and 2017, he was 1024  
the recipient of the prestigious Established Career Fellowship from the 1025  
Engineering and Physical Sciences Research Council (EPSRC) within 1026  
Information and Communications Technology in the U.K. In 2014, he was 1027  
selected by EPSRC as one of ten Recognising Inspirational Scientists and 1028  
Engineers Leaders in the U.K. He was the co-recipient of the EURASIP Best 1029  
Paper Award for the *Journal on Wireless Communications and Networking* 1030  
in 2015, and co-recipient of the Jack Neubauer Memorial Award of the IEEE 1031  
VEHICULAR TECHNOLOGY SOCIETY. In 2016, he was a recipient of the 1032  
outstanding achievement award from the International Solid State Lighting 1033  
Alliance. He was the co-recipient of recent Best Paper Awards at VTC, 1034  
2013, VTC 2015, ICC 2016, and ICC 2017. He is currently an Editor of the 1035  
IEEE TRANSACTIONS ON COMMUNICATIONS and the IEEE JOURNAL OF 1036  
LIGHTWAVE TECHNOLOGIES. 1037

# Physical-Layer Security in Multiuser Visible Light Communication Networks

Liang Yin and Harald Haas, *Senior Member, IEEE*

**Abstract**—In this paper, we study the physical-layer security in a 3-D multiuser visible light communication (VLC) network. The locations of access points (APs) and mobile users are modeled as two 2-D, independent and homogeneous Poisson point processes at distinct heights. Using mathematical tools from stochastic geometry, we provide a new analytical framework to characterize the secrecy performance in multiuser VLC networks. Closed-form results for the outage probability and the ergodic secrecy rate are derived for networks without AP cooperation. Considering the cooperation among APs, we give tight lower and upper bounds on the secrecy outage probability and the ergodic secrecy rate. To further enhance the secrecy performance at the legitimate user, a disk-shaped secrecy protected zone is implemented in the vicinity of the transmit AP. Based on the obtained results, it is shown that cooperating neighboring APs in a multiuser VLC network can bring performance gains on the secrecy rate, but only to a limited extent. We also show that building an eavesdropper-free protected zone around the AP significantly improves the secrecy performance of legitimate users, which appears to be a promising solution for the design of multiuser VLC networks with high security requirements.

**Index Terms**—Visible light communication, secrecy capacity, physical-layer security, poisson point process, stochastic geometry.

## I. INTRODUCTION

BY UTILIZING the existing lighting infrastructure and shifting the communication frequency to the visible spectrum, visible light communication (VLC) [1]–[3] has recently emerged as a promising candidate for future high-speed broadband communications, which could effectively alleviate the spectrum congestion issue in current radio frequency (RF) based wireless systems. Recent advances have also led to the standardization of short-range wireless optical communication using VLC for local and metropolitan area networks [4], which serves as a major step towards its commercialization in the near future. Compared to RF communication, VLC has the following main advantages: 1) VLC builds upon existing lighting devices and operates on the license-free spectrum so that it has lower implementation cost; 2) VLC can operate safely in electromagnetic sensitive areas, where RF is intrinsically prohibited; 3) VLC networking can be designed in

addition to existing heterogeneous wireless networks because it receives zero interference from, and adds zero interference to its RF counterparts; 4) Based on the property that visible light does not penetrate through opaque objects, the communication bandwidth in one room can be efficiently reused in other rooms to obtain a high frequency reuse factor and hence a high area spectral efficiency; 5) Indoor VLC typically achieves higher physical-layer security since the transmitted signal is confined within the room.

The broadcast property of VLC has been utilized in many novel designs of multiuser VLC networks [5]–[7]. However, it also causes potential concerns to legitimate users and network administrators regarding the information privacy and confidentiality, especially in public areas, such as train stations and libraries. From an information-theoretic point of view, the physical-layer security was pioneered by Wyner for proposing the wiretap channel [8]: a channel in which an eavesdropper receives a degraded version of the transmitted signal. The degraded wiretap channel was later extended to the non-degraded broadcast channel by Csiszár and Körner [9]. In their seminal work, it is shown that perfect secrecy can be achieved as long as the legitimate user has a less degraded channel than the eavesdropper, and the secrecy capacity is derived as the difference between the information capacity for the two users. Typical security enhancement techniques that are implemented at upper layers of the communication chain include password protection and user admission control. Physical-layer security, on the other hand, exploits the randomness of the noise and the wireless communication channel to limit the amount of legitimate information to be detected by unauthorized eavesdroppers [8], [9].

Different from point-to-point communication, studying the secrecy performance in a large-scale wireless network requires not only the knowledge of locations of legitimate users but also the knowledge of locations of eavesdropping users that may interact with legitimate users. Initial works that characterize the secrecy performance in multiuser wireless networks rely on the secrecy graph model to study the node connectivity [10], [11] and the maximum secrecy rate [12], from an information-theoretic perspective. Following these works, the secrecy rate per source-destination pair was investigated in [13] by characterizing the secrecy capacity scaling laws in a wireless network. Moving from network information theory, recent works have evaluated the secrecy performance in multiuser wireless networks using mathematical tools from stochastic geometry [14], [15]. It should be noted that works in [8]–[15] are all focused on RF based wireless networks.

Manuscript received February 22, 2017; revised July 15, 2017; accepted September 16, 2017. This work was supported by the U.K. Engineering and Physical Sciences Research Council under Grant EP/K008757/1. (Corresponding author: Liang Yin.)

The authors are with the School of Engineering, Institute for Digital Communications, Li-Fi Research and Development Centre, University of Edinburgh, Edinburgh EH9 3JL, U.K. (e-mail: l.yin@ed.ac.uk; h.haas@ed.ac.uk).

Color versions of one or more of the figures in this paper are available online at <http://ieeexplore.ieee.org>.

Digital Object Identifier 10.1109/JSAC.2017.2774429

Different from RF communication, which is typically modeled as a Gaussian broadcast channel with an average power constraint at the transmitter side, VLC typically uses intensity modulation and direct detection (IM/DD) due to the use of inexpensive light-emitting diodes (LEDs) and photodiodes (PDs) as the optical transmitter and receiver, respectively. In VLC, since the signal is modulated onto the intensity of the emitted light, it must satisfy average, peak as well as non-negative amplitude constraints, that are imposed by the dynamic range of typical LEDs and practical illumination requirements [6], [16]–[18]. Although typical LEDs have a nonlinear electrical-to-optical (E/O) transfer characteristic, this nonlinearity can be successfully compensated by pre-distortion techniques [19]. Also, since the wavelength of visible light is hundreds of nanometers while the detection area of a typical PD is millions of square wavelengths, this spatial diversity essentially prevents the “multipath fading” effect in the VLC channel. Due to these fundamental differences, results on the secrecy capacity obtained for RF networks can not be directly applied to VLC networks.

Since the secrecy capacity is related to the information capacity of the communication channel [8], [9], before determining the secrecy capacity in VLC networks it is essential to obtain the information capacity of the VLC channel with average, peak and non-negative constraints. However, to the best of authors’ knowledge, the exact information capacity of the VLC channel with such constraints still remains unknown, even for the simplest single-input single-output (SISO) case, despite some lower and upper bounds have been derived [16]–[18]. By considering one transmitter, one legitimate user and one eavesdropper in a VLC system, lower and upper bounds on the secrecy capacity of the amplitude-constrained Gaussian wiretap channel was recently studied in [20], with the use of the derived capacity lower and upper bounds in [16]. In the same work [20], beamforming was also utilized to improve the secrecy capacity for the multiple-input single-output (MISO) VLC channel. Following this, the optimal beamformer design problem subject to amplitude constraints was further studied in [21]. The secrecy performance in a single-cell VLC system with only one AP was studied in [22]. However, the randomness of legitimate users as well as eavesdroppers and, more importantly, the interactions between them, have not been fully characterized when analyzing the secrecy performance in a random multiuser VLC network.

### A. Approaches and Contributions

In this work, we aim to characterize the secrecy performance in an indoor multiuser VLC network by considering the unique properties of the VLC channel as well as the network layout, that differ from typical RF networks. Our approach builds upon a proposed three-dimensional network model with two independent random topologies for the VLC APs and mobile users. Specifically, the VLC APs are modeled by a two-dimensional homogeneous Poisson point process (PPP) in the ceiling, while the locations of users, that include both legitimate users and eavesdroppers, are modeled by another independent two-dimensional homogeneous PPP at

the user plane. To separate eavesdroppers from legitimate users, the locations of random eavesdroppers are obtained from a thinned PPP. Despite the grid-like deployment of LEDs in typical offices, the following observations indicate that a stochastic model may be required to accurately capture the distribution of APs in a VLC network. First, more and more LEDs with built-in motion-detection sensors are deployed in public spaces in order to reduce energy consumption. In this case, some of the LEDs will be temporally switched off when they are not required to provide illumination. Second, the distribution of ceiling lights is not necessarily equivalent to the distribution of APs in a VLC network because not necessarily all of the ceiling lights are simultaneously operating in the communication mode, i.e., some of the ceiling lights may operate in the illumination mode only when no data traffic is demanded from them. In these scenarios, the distribution of APs can not be accurately modeled by the grid model. Instead, a stochastic thinning process built upon the grid-like deployment of LEDs is more accurate, where the activeness/idleness of each AP is determined by a time-varying probability distribution function (PDF). However, finding the PDF of activeness/idleness of the LED requires full knowledge of the users’ movement and handover characteristics, which is generally complicated and not analytically tractable. In order to derive analytically tractable results, the PPP model is assumed in this work. For completeness, we also compare the secrecy performance between the PPP model and the grid model and provide a method of applying the derived analytical results to estimate the secrecy performance in a conventional grid-like VLC network.

The main contributions of this paper are as follows:

- 1) When the legitimate user is served by the nearest AP in its vicinity, we derive the distribution function of the secrecy rate of a typical legitimate user, based on which secrecy outage probability and ergodic secrecy rate are obtained. To provide further insights into the secrecy performance with different network parameters, lower and upper bounds on the secrecy outage probability as well as on the ergodic secrecy rate are given.
- 2) We enhance the secrecy performance by implementing AP cooperation in a multiuser VLC network, and give lower and upper bounds on the secrecy outage probability and the ergodic secrecy rate. The derived analytical bounds are found to be reasonably tight in general and become tighter when the density of eavesdroppers becomes larger.
- 3) To further enhance the secrecy performance for legitimate users, we introduce a disk-shaped secrecy protected zone around the AP in a multiuser VLC network, in which the presence of eavesdroppers is prohibited. In this scenario, the secrecy outage probability and the ergodic secrecy rate are derived. The impact of designing the protected zone with different sizes on the secrecy performance is also investigated.

The remainder of this paper is organized as follows. In Section II, we introduce a three-dimensional link model for multiuser VLC networks and formulate the information-theoretic secrecy rate expression based on a close



203 approximation of the channel capacity. The secrecy outage  
 204 probability and the ergodic secrecy rate with/without the AP  
 205 cooperation are derived in Section III. We extend the analysis  
 206 on the secrecy performance in Section IV by implementing a  
 207 disk-shaped protected zone. Simulation results and discussions  
 208 are provided in Section V. Finally, concluding remarks are  
 209 given in Section VI.

## 210 II. SYSTEM MODEL

### 211 A. Poisson Network Model

212 We consider a downlink transmission scenario of a multiuser  
 213 VLC network with the presence of both legitimate users and  
 214 eavesdroppers inside a three-dimensional space. The VLC  
 215 APs are vertically fixed, since they are attached to the room  
 216 ceiling, and their horizontal positions are modeled by a  
 217 two-dimensional homogeneous PPP  $\Phi_a$  with density  $\lambda_a$ ,  
 218 in nodes per unit area. Similarly, mobile users are assumed to  
 219 be at a fixed height and their horizontal positions are modeled  
 220 by another independent two-dimensional homogeneous PPP  
 221  $\Phi_u$  with density  $\lambda_u$ . The vertical distance between the AP  
 222 plane and the user plane is denoted by  $L$ . After adding an  
 223 additional user at the room center,<sup>1</sup> the new point process  
 224 for mobile users becomes  $\Phi_u \cup \{0\}$ . Slivnyak's theorem states  
 225 that adding a user into  $\Phi_u$  is equivalent to conditioning  $\Phi_u$   
 226 on the added point, and this process does not change the  
 227 distribution of  $\Phi_u$  [23]. Therefore, the added user at the origin  
 228 can be treated as the *typical* legitimate user in the study  
 229 since it can reflect the spatial average of the performance of  
 230 all legitimate users in the network. Among all of the users,  
 231 there exist malicious eavesdroppers that could compromise  
 232 the transmission privacy of ongoing legitimate links, due to  
 233 the broadcast nature of the VLC channel. Since eavesdroppers  
 234 typically disguise as legitimate users, it is uncertain whether  
 235 a random user  $u \in \Phi_u$  is a legitimate user or an eavesdropper.  
 236 Therefore, it is assumed that  $u$  is an eavesdropper with  
 237 probability  $p_e$  and that  $u$  is a legitimate user with probability  
 238  $1 - p_e$ . This thinned realization of  $\Phi_u$  gives the point process  
 239 for eavesdroppers,  $\Phi_e$ , which is also a homogeneous PPP  
 240 whose density can be found as  $\lambda_e = p_e \lambda_u$  [23]. Furthermore,  
 241 it is assumed that eavesdroppers do not collude with each other  
 242 so that each eavesdropper needs to decode any confidential  
 243 messages sent to legitimate users individually. An example of  
 244 the described multiuser VLC network is depicted in Fig. 1.

245 A complete VLC channel includes both the line-of-  
 246 sight (LOS) link and non-line-of-sight (NLOS) links, that are  
 247 caused by light reflections from interior surfaces. However,  
 248 in a typical indoor lighting environment, the sum signal power  
 249 carried by NLOS components is significantly weaker than that  
 250 carried by the LOS link [1], [24], [25]. Therefore, we will  
 251 only focus on the LOS link in the following analysis in  
 252 order to obtain tractable analytical results. The VLC APs  
 253 are assumed to have a Lambertian radiation profile whose  
 254 Lambertian order is  $m = -1/\log_2(\cos(\Phi_{1/2}))$ , where  $\Phi_{1/2}$

<sup>1</sup>The room center is also called the origin. We use both expressions inter-  
 changeably throughout the paper since the room center has more geographical  
 meanings while the origin has more mathematical meanings when we apply  
 stochastic geometry tools in the theoretical analysis.

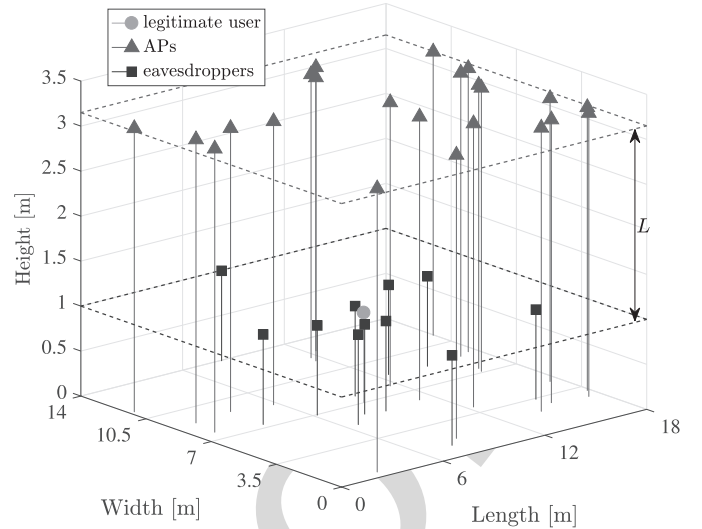


Fig. 1. Random network model: the legitimate user of interest is placed at the room center; VLC APs are randomly distributed in the ceiling according to a homogeneous PPP  $\Phi_a$ ; and eavesdroppers are randomly distributed on the same plane as the legitimate user, following a homogeneous PPP  $\Phi_e$ . In this example, an indoor VLC network of size  $18 \times 14 \times 3.5$  m<sup>3</sup> is shown.

255 denotes the semi-angle of the LED. The PD equipped at each  
 256 user is assumed to be facing vertically upwards with a field-of-  
 257 view (FOV) of  $\Psi_{\text{fov}}$ . For each VLC link, the optical channel  
 258 direct current (DC) gain is given by [26]:

$$259 \quad h = \frac{(m+1)A\eta}{2\pi d^2} \cos^m(\phi) T(\psi) g(\psi) \cos(\psi), \quad (1)$$

260 where  $A$  denotes the effective detection area of the PD;  $\eta$   
 261 is the responsivity of the PD;  $\phi$  and  $\psi$  are the angle of  
 262 irradiance and the angle of incidence of the optical link,  
 263 respectively;  $T(\psi)$  represents the gain of the optical filter used  
 264 at the receiver; and  $g(\psi)$  represents the gain of the optical  
 265 concentrator. The optical concentrator gain is given by [26]:

$$266 \quad g(\psi) = \begin{cases} \frac{n^2}{\sin^2(\Psi_{\text{fov}})}, & 0 \leq \psi \leq \Psi_{\text{fov}} \\ 0, & \psi > \Psi_{\text{fov}} \end{cases}, \quad (2)$$

267 where  $n$  is the reflective index of the optical concentrator, and  
 268 it is defined as the ratio of the speed of light in vacuum and  
 269 the phase velocity of light in the optical material. For visible  
 270 light, the typical value for  $n$  varies between 1 and 2.

271 Consider the communication link from an AP  $x \in \Phi_a$  to  
 272 an eavesdropper  $e \in \Phi_e$ . Based on the geometry [7] of the  
 273 VLC link, it is easy to obtain  $d = \sqrt{\|e-x\|^2 + L^2}$ ,  $\cos(\phi) =$   
 274  $L/\sqrt{\|e-x\|^2 + L^2}$  and  $\cos(\psi) = L/\sqrt{\|e-x\|^2 + L^2}$ .  
 275 Therefore, the received optical power at eavesdropper  $e$  from  
 276 AP  $x$  can be written as:

$$277 \quad P_{\text{rx}}(x, e) = h P_{\text{tx}} \\ 278 \quad = \frac{(m+1)A\eta T(\psi) g(\psi) L^{m+1}}{2\pi(\|e-x\|^2 + L^2)^{\frac{m+3}{2}}} P_{\text{tx}}, \quad (3)$$

279 where  $P_{\text{tx}}$  denotes the transmit optical power of the AP.  
 280 Similarly, the received signal power at the legitimate user can  
 281 be written as  $P_{\text{rx}}(x, o)$ , where  $o$  representing the origin is the  
 282 location of the typical user of interest.

### B. Secrecy Capacity Formulation

The classic Shannon equation does not apply to VLC because of the average, peak and non-negative constraints on the modulated optical signal. Although the exact capacity of the VLC channel remains unknown, several upper and lower bounds have been derived [16]–[18]. Based on the capacity lower bound derived in [16], the exact channel capacity of VLC can be written as:

$$C = \frac{1}{2} \log_2 \left( 1 + \frac{\exp(1)P_{\text{rx}}^2}{2\pi\sigma_n^2} \right) + \epsilon \left( \frac{P_{\text{rx}}}{\sigma_n} \right), \quad (4)$$

where  $\epsilon$ , as a function of the received optical-signal-to-noise ratio (OSNR)  $P_{\text{rx}}/\sigma_n$ , represents a positive capacity gap between the exact channel capacity and the analytical lower bound [16], and  $\sigma_n^2$  represents the total power of noise processes at the receiver. Note that inside the receiver circuit the dominant noise sources are the thermal noise and shot noise [1], [25]. The thermal noise is mainly caused by the preamplifier circuits while the shot noise originates mainly from the ambient light and/or other light sources. The signal-dependent shot noise, on the other hand, is relatively small, and hence its effect can be ignored. The overall noise process is generally well modeled as the additive white Gaussian noise (AWGN) [1], [25]. As the legitimate user and eavesdroppers may use different grades of receivers, for example, PDs with different detection areas and/or bandwidths, they are subject to different levels of receiver noise and are capable of detecting signals with different amplifying gains. Without loss of generality, the choice of different grades of receivers can be accounted for in the system model by assigning different noise variances at the legitimate user and the eavesdropper. Based on this, we denote by  $\sigma_{\text{nb}}^2$  and  $\sigma_{\text{ne}}^2$  the noise variance at the legitimate user and the noise variance at the eavesdropper, respectively. Unlike RF channels whose input signals are subject to an average power constraint [29], VLC channels require the input signals to satisfy a peak amplitude (optical power) constraint. This makes it challenging to obtain closed-form expressions for the secrecy capacity of a VLC link, even for the simplest SISO case [20], [30]. Therefore, in the following analysis we focus on a tight achievable lower bound on the secrecy capacity [20]:

$$C_s \geq [C_b - C_e]^+ = \underline{C}_s, \quad (5)$$

where  $[a]^+ = \max\{a, 0\}$ ;  $C_s$  represents the exact secrecy capacity;  $\underline{C}_s$  represents the tight lower bound on the secrecy capacity given by the right-hand side of (5);  $C_b$  is the channel capacity of the legitimate link; and  $C_e$  is the channel capacity of the eavesdropper's link.

### III. SECRECY RATE IN RANDOM VLC NETWORKS

#### A. Nearest AP to Serve the Legitimate User

Without AP cooperation, the nearest AP is typically assumed to serve a mobile user in the VLC network in order to maximize the information rate of the communication link. As a result, based on (4), the capacity of the legitimate link can be written as  $C_b = \max_{x \in \Phi_a} \frac{1}{2} \log_2(1 + \exp(1)P_{\text{rx}}^2(x, o)/2\pi\sigma_{\text{nb}}^2) + \epsilon(P_{\text{rx}}(x, o)/\sigma_{\text{nb}}) = \frac{1}{2} \log_2(1 + \exp(1)P_{\text{rx}}^2(x_0, o)/2\pi\sigma_{\text{nb}}^2) + \epsilon(P_{\text{rx}}(x_0, o)/\sigma_{\text{nb}})$ , where  $x_0$  represents the location of the

nearest AP to the origin. Since it is assumed that eavesdroppers do not collude, the secrecy performance of the legitimate user is limited by the eavesdropper with the highest OSNR. Therefore, the lower bound on the secrecy capacity at the typical legitimate user is formulated as:

$$\underline{C}_s = \left[ \frac{1}{2} \log_2 \left( 1 + \frac{\exp(1)P_{\text{rx}}^2(x_0, o)}{2\pi\sigma_{\text{nb}}^2} \right) - \frac{1}{2} \log_2 \left( 1 + \frac{\exp(1)P_{\text{rx}}^2(x_0, e^*(x_0))}{2\pi\sigma_{\text{ne}}^2} \right) + \epsilon \left( \frac{P_{\text{rx}}(x_0, o)}{\sigma_{\text{nb}}} \right) - \epsilon \left( \frac{P_{\text{rx}}(x_0, e^*(x_0))}{\sigma_{\text{ne}}} \right) \right]^+, \quad (6)$$

where  $e^*(x_0)$  denotes the horizontal distance from AP  $x_0$  to the nearest eavesdropper. Given that the legitimate user is connected to AP  $x$ , the general solution for  $e^*(x)$ , denoting the horizontal distance between AP  $x$  and the strongest eavesdropper, can be obtained by finding the location of the eavesdropper  $e \in \Phi_e$  that receives the strongest signal power:

$$\begin{aligned} e^*(x) &= \arg \max_{e \in \Phi_e} P_{\text{rx}}(x, e) \\ &= \arg \min_{e \in \Phi_e} \|e - x\|, \end{aligned} \quad (7)$$

where the last step is obtained based on the monotonic property of (3). By utilizing fractional frequency reuse [28] or orthogonal multiple access techniques, the achievable data rate can be quantified through the received signal-to-noise ratio (SNR) without the side effect of co-channel interference (CSI). As a result, OSNR of  $P_{\text{rx}}/\sigma_n > 30$  dB can be achieved at typical illumination levels [25], [27], where  $\epsilon(P_{\text{rx}}/\sigma_n)$  is found to be comparatively small [16]–[18]. Therefore, we focus on the high OSNR regime, where  $\epsilon(P_{\text{rx}}(x_0, o)/\sigma_{\text{nb}}) \ll 1/2 \log_2(\exp(1)P_{\text{rx}}^2(x_0, o)/2\pi\sigma_{\text{nb}}^2)$  and  $\epsilon(P_{\text{rx}}(x_0, e^*(x_0))/\sigma_{\text{ne}}) \ll 1/2 \log_2(\exp(1)P_{\text{rx}}^2(x_0, e^*(x_0))/2\pi\sigma_{\text{ne}}^2)$ . Based on this, (6) can be further approximated to:

$$\underline{C}_s \approx \left[ \frac{1}{2} \log_2 \left( \frac{P_{\text{rx}}^2(x_0, o)}{P_{\text{rx}}^2(x_0, e^*(x))} \right) + \log_2 \left( \frac{\sigma_{\text{ne}}}{\sigma_{\text{nb}}} \right) \right]^+ = R_s. \quad (8)$$

To distinguish from the exact secrecy capacity, we define in (8)  $R_s$  as the achievable secrecy rate. Due to the lack of the complete knowledge of the exact secrecy capacity  $C_s$ , the secrecy rate  $R_s$  is of interest in this paper. It is shown in (8) that a non-negative secrecy rate can only be achieved when the legitimate user achieves a higher SNR than the strongest eavesdropper. In the case that a eavesdropper receives signals from a less-degraded link than the legitimate user, the achievable secrecy rate drops to zero. It can also be seen from (8) that when the legitimate user and the eavesdropper use different grades of receivers, the achieved secrecy capacity at the legitimate user is offset by a constant, whose value is proportional to the logarithm of  $\sigma_{\text{ne}}/\sigma_{\text{nb}}$ . Therefore, without loss of generality,  $\sigma_{\text{nb}} = \sigma_{\text{ne}}$  is assumed in the following analysis.

*Theorem 1:* When the legitimate user is served by the nearest AP in its vicinity, the cumulative distribution function (CDF) of the secrecy rate  $R_s$  is given by:

$$F_{R_s}(v) = 1 - \frac{1}{1 + \frac{\lambda_e}{\lambda_a} 4^{\frac{v}{m+3}}} \exp \left( -\pi \lambda_e \left( 4^{\frac{v}{m+3}} - 1 \right) L^2 \right), \quad (9)$$

where  $v \geq 0$ .

*Proof:* According to (8), we have  $R_s \geq 0$ . Therefore, the CDF of the secrecy rate  $R_s$  can be calculated by:

$$\begin{aligned} F_{R_s}(v) &= \mathbb{P}[R_s \leq v] \\ &= \mathbb{P}\left[\frac{P_{rx}^2(x_0, o)}{P_{rx}^2(x_0, e^*(x_0))} \leq 4^v\right] \\ &= \mathbb{P}\left[\|e^*(x_0) - x_0\| \leq \sqrt{\beta x_0^2 + (\beta - 1)L^2}\right], \end{aligned} \quad (10)$$

where  $\beta = 4^{v/(m+3)}$ . Since the legitimate user is served by the nearest AP, the PDF of  $x_0$  is [31]:

$$f_{x_0}(x_0) = 2\pi \lambda_a x_0 \exp\left(-\pi \lambda_a x_0^2\right). \quad (11)$$

When conditioned on distance  $x_0$ , (10) is the probability that no eavesdroppers exist within a circle, which is centered at  $x_0$  and has a radius of  $\sqrt{\beta x_0^2 + (\beta - 1)L^2}$ . Such probability can be calculated using the void probability of PPP [32]. As a result, (10) can be calculated as:

$$\begin{aligned} F_{R_s}(v) &= \mathbb{E}_{x_0} \left[ \mathbb{P} \left[ \|e^*(x_0) - x_0\| \leq \sqrt{\beta x_0^2 + (\beta - 1)L^2} \mid x_0 \right] \right] \\ &= \int_0^\infty \mathbb{P} \left[ \|e^*(x_0) - x_0\| \leq \sqrt{\beta x_0^2 + (\beta - 1)L^2} \mid x_0 \right] f_{x_0}(x_0) dx_0 \\ &= \int_0^\infty \left( 1 - \exp\left(-\pi \lambda_e \left(\beta x_0^2 + (\beta - 1)L^2\right)\right) \right) 2\pi \lambda_a x_0 \\ &\quad \times \exp\left(-\pi \lambda_a x_0^2\right) dx_0 \\ &= 1 - \frac{1}{1 + \frac{\lambda_e}{\lambda_a} \beta} \exp\left(-\pi \lambda_e (\beta - 1) L^2\right). \end{aligned} \quad (12)$$

After plugging  $\beta = 4^{v/(m+3)}$  into (12), we obtain (9). ■

*Corollary 1:* When the legitimate user is served by the  $n$ -th nearest AP in its vicinity, the CDF of the secrecy rate is:

$$F_{R_s}(v) = 1 - \left( \frac{1}{1 + \frac{\lambda_e}{\lambda_a} 4^{\frac{v}{m+3}}} \right)^n \exp\left(-\pi \lambda_e \left(4^{\frac{v}{m+3}} - 1\right) L^2\right), \quad (13)$$

where  $v \geq 0$ .

*Proof:* The distance distribution of the legitimate user to the  $n$ -th nearest AP is given by [31]:

$$f_{x_n}(x_n) = \frac{2(\pi \lambda_a x_n^2)^n}{x_n \Gamma(n)} \exp\left(-\pi \lambda_a x_n^2\right). \quad (14)$$

By using (14) and following similar steps as in (12), (13) can be obtained. ■

The secrecy outage probability, denoted by  $p_{so}$ , is defined as the probability that the secrecy rate is below a target secrecy rate  $\bar{R}_s$ . Mathematically, it is formulated as:

$$p_{so} = \mathbb{P}[R_s \leq \bar{R}_s] = F_{R_s}(\bar{R}_s), \quad (15)$$

which can be obtained directly from Theorem 1.

*Corollary 2:* When the legitimate user is served by the nearest AP in its vicinity, the secrecy outage probability is lower bounded by:

$$p_{so}^{\text{LB}} = 1 - \exp\left(-\pi \lambda_e \left(4^{\frac{\bar{R}_s}{m+3}} - 1\right) L^2\right), \quad (16)$$

when the density of VLC APs approaches infinity.

*Proof:* (16) can be obtained from  $p_{so}^{\text{LB}} = \lim_{\lambda_a \rightarrow \infty} p_{so}$ . ■

Theorem 1 and Corollary 2 provide an important guideline for the design of VLC networks: installing more VLC APs can help decrease the secrecy outage probability of a typical legitimate user; however, when the density of APs reaches a certain level, further increasing the density of APs is not meaningful since it can no longer enhance the secrecy performance. In other words, it is impossible for a legitimate user in the network to simultaneously achieve a target secrecy rate  $\bar{R}_s$  and have an outage probability lower than  $p_{so}^{\text{LB}}(\bar{R}_s)$ . Given a target secrecy rate  $\bar{R}_s$  and a target outage probability  $\bar{p}_{so} > p_{so}^{\text{LB}}(\bar{R}_s)$ , this requirement can be achieved by installing more APs in the network so that the density of APs satisfies  $\lambda_a \geq \lambda_e (1 - \bar{p}_{so}) 4^{\frac{\bar{R}_s}{m+3}} / (\bar{p}_{so} - p_{so}^{\text{LB}}(\bar{R}_s))$ . From (9) and (16), it is shown that reducing the semi-angle of the LED, or equivalently increasing the Lambertian order, can also help improve the secrecy performance of the network. Nevertheless, the actual choice of the semi-angle of the LED should also satisfy the illumination requirement.

*Theorem 2:* When the legitimate user is served by the nearest AP in its vicinity, the ergodic secrecy rate at the legitimate user is:

$$\begin{aligned} \mathbb{E}[R_s] &= \frac{m+3}{\ln(4)} \left[ \exp\left(\pi(\lambda_e + \lambda_a)L^2\right) \text{Ei}\left(-\pi(\lambda_e + \lambda_a)L^2\right) \right. \\ &\quad \left. - \exp\left(\pi\lambda_e L^2\right) \text{Ei}\left(-\pi\lambda_e L^2\right) \right], \end{aligned} \quad (17)$$

where  $\text{Ei}(a) = -\int_{-a}^\infty \exp(-t)/t dt$  is the exponential integral function [33].

*Proof:* The ergodic secrecy rate can be calculated based on the CDF of  $R_s$ :

$$\begin{aligned} \mathbb{E}[R_s] &= \int_0^\infty (1 - F_{R_s}(v)) dv \\ &= \frac{m+3}{\ln(4)} \int_1^\infty \frac{1}{\beta \left(1 + \frac{\lambda_e}{\lambda_a} \beta\right)} \exp\left(-\pi \lambda_e (\beta - 1) L^2\right) d\beta \\ &= \frac{m+3}{\ln(4)} \left[ \int_1^\infty \frac{\exp\left(-\pi \lambda_e (\beta - 1) L^2\right)}{\beta} d\beta \right. \\ &\quad \left. - \int_1^\infty \frac{\exp\left(-\pi \lambda_e (\beta - 1) L^2\right)}{\beta + \frac{\lambda_a}{\lambda_e}} d\beta \right], \end{aligned} \quad (18)$$

where the integration variable has been changed from  $v$  to  $\beta$ . After applying [33, eq. 3.351.5], the first integration in (18) can be calculated as:

$$\int_1^\infty \frac{\exp\left(-\pi \lambda_e (\beta - 1) L^2\right)}{\beta} d\beta = -\exp\left(\pi \lambda_e L^2\right) \text{Ei}\left(-\pi \lambda_e L^2\right). \quad (19)$$

After applying [33, eq. 3.352.2], the second integration in (18) can be calculated as:

$$\begin{aligned} &\int_1^\infty \frac{\exp\left(-\pi \lambda_e (\beta - 1) L^2\right)}{\beta + \frac{\lambda_a}{\lambda_e}} d\beta \\ &= -\exp\left(\pi(\lambda_e + \lambda_a)L^2\right) \text{Ei}\left(-\pi(\lambda_e + \lambda_a)L^2\right). \end{aligned} \quad (20)$$

After plugging (19) and (20) into (18), (17) is obtained. ■

468 *Corollary 3:* When the legitimate user is served by the  
469 nearest AP in its vicinity, the ergodic secrecy rate at the  
470 legitimate user is upper bounded by:

$$471 \quad R_s^{\text{UB}} = \frac{m+3}{\ln(4)} \left( -\exp\left(\pi \lambda_e L^2\right) \text{Ei}\left(-\pi \lambda_e L^2\right) \right). \quad (21)$$

472 *Proof:* The upper bound on the secrecy rate can be  
473 obtained from  $R_s^{\text{UB}} = \lim_{\lambda_a \rightarrow \infty} \mathbb{E}[R_s]$ . Based on the equality

$$474 \quad \lim_{\lambda_a \rightarrow \infty} \exp\left(\pi(\lambda_e + \lambda_a)L^2\right) \text{Ei}\left(-\pi(\lambda_e + \lambda_a)L^2\right) = 0, \quad (22)$$

475 we obtain (21). ■

476 Theorem 2 and Corollary 3 indicate that increasing the density  
477 of VLC APs can help enhance the ergodic secrecy rate of  
478 a typical legitimate user. However, when the density of APs  
479 exceeds a certain level, installing more APs can not enhance  
480 the ergodic secrecy rate any further. While satisfying the  
481 illumination requirement, using LEDs with a smaller semi-  
482 angle can increase the ergodic secrecy rate of a typical user.  
483 Specifically, it can be seen from (17) and (21) that a linear  
484 relationship exists between the ergodic secrecy rate and the  
485 Lambertian order  $m$ . Given the choice of LEDs, the maximum  
486 ergodic secrecy rate can not exceed the upper bound given  
487 in (21). To achieve a target ergodic secrecy rate  $\bar{R}_s$ , whose  
488 value is smaller than  $R_s^{\text{UB}}$ , the density of APs needs to  
489 exceed  $\lambda_a^*$ , where  $\lambda_a^*$  is the numerical solution for  $\lambda_a$  to equa-  
490 tion  $\exp\left(\pi(\lambda_e + \lambda_a)L^2\right) \text{Ei}\left(-\pi(\lambda_e + \lambda_a)L^2\right) = \ln(4)\bar{R}_s /$   
491  $(m+3) + \exp\left(\pi \lambda_e L^2\right) \text{Ei}\left(-\pi \lambda_e L^2\right)$ .

### 492 B. Optimal AP to Serve the Legitimate User

493 Due to the randomness of eavesdroppers, it is not always  
494 optimal to serve the legitimate user with the nearest AP. For  
495 example, if the eavesdropper is close to the nearest AP around  
496 the legitimate user but far away from the second nearest  
497 AP around the legitimate user, selecting the second nearest  
498 AP to serve the legitimate user may yield a higher secrecy  
499 rate. Therefore, with the cooperation among APs, the secrecy  
500 performance at legitimate users can be further enhanced.  
501 However, it should be noted that selecting the optimal AP to  
502 serve legitimate users requires the knowledge of the location  
503 information of all eavesdroppers at the central controller,  
504 which can be achieved with indoor sensing and localization  
505 technologies. Despite the additional implementation and compu-  
506 tation complexity, this optimal scheme yields an enhanced  
507 secrecy rate, which is useful for network designers to quantify  
508 the secrecy performance provided by the nearest AP and  
509 optimal AP and to decide which scheme is more suitable for  
510 practical implementations. When the optimal AP is selected  
511 to serve the legitimate user, the secrecy rate is formulated as:

$$512 \quad R_s = \left[ \max_{x \in \Phi_a} \left\{ \frac{1}{2} \log_2 \left( \frac{P_{\text{rx}}^2(x, o)}{P_{\text{rx}}^2(x, e^*(x))} \right) \right\} \right]^+. \quad (23)$$

513 Due to the intractability of the secrecy rate expression given  
514 in (23), the distribution function of  $R_s$  is hard to obtain. In the  
515 following, we provide two analytical bounds on the CDF of the  
516 secrecy rate.

517 *Corollary 4:* With the cooperation among VLC APs,  
518 the CDF of the secrecy rate at the typical legitimate user is  
519 lower bounded by:

$$520 \quad F_{R_s}(v) \geq \exp\left(-\frac{\lambda_a}{\lambda_e} 4^{-\frac{v}{m+3}} \exp\left(-\pi \lambda_e \left(4^{\frac{v}{m+3}} - 1\right) L^2\right)\right), \quad (24)$$

521 and is upper bounded by:

$$522 \quad F_{R_s}(v) \leq 1 - \frac{1}{1 + \frac{\lambda_e}{\lambda_a} 4^{\frac{v}{m+3}}} \exp\left(-\pi \lambda_e \left(4^{\frac{v}{m+3}} - 1\right) L^2\right). \quad (25)$$

523 *Proof:* With the cooperation of VLC APs, the CDF of the  
524 secrecy rate can be calculated with the help of the probability  
525 generating functional (PGFL) of the PPP [23]:

$$526 \quad \begin{aligned} 527 \quad F_{R_s}(v) &= \mathbb{P} \left[ \max_{x \in \Phi_a} \left\{ \frac{1}{2} \log_2 \left( \frac{P_{\text{rx}}^2(x, o)}{P_{\text{rx}}^2(x, e^*(x))} \right) \right\} \leq v \right] \\ 528 &= \mathbb{P} \left[ \frac{1}{2} \log_2 \left( \frac{P_{\text{rx}}^2(x, o)}{P_{\text{rx}}^2(x, e^*(x))} \right) \leq v, \forall x \in \Phi_a \right] \\ 529 &= \mathbb{E}_{\Phi_e} \left[ \mathbb{E}_{\Phi_a} \left[ \prod_{x \in \Phi_a} \mathbf{1} \left( \|e-x\| \leq \sqrt{\beta L^2 + (\beta-1)L^2} \right) \right] \right] \\ 530 &= \mathbb{E}_{\Phi_e} \left[ \exp \left[ -\lambda_a \int_{\mathbb{R}^2} \mathbf{1} \left[ \|e-x\| > \sqrt{\beta L^2 + (\beta-1)L^2} \mid x \right] dx \right] \right], \end{aligned} \quad (26)$$

531 where  $\mathbf{1}(\mathcal{A}) = 1$  with event  $\mathcal{A}$  being true, and zero otherwise.  
532 Based on Jensen's inequality, the lower bound can be calcu-  
533 lated as:

$$534 \quad F_{R_s}(v) \geq \exp \left[ -2\pi \lambda_a \int_0^\infty \mathbb{P} \left[ \|e-x\| > \sqrt{\beta x^2 + (\beta-1)L^2} \mid x \right] \right. \\ \left. \times x dx \right]. \quad (27)$$

535 After calculating the integration part in (27), the lower bound  
536 result in Corollary 4 is obtained. The upper bound can be  
537 obtained straightforwardly from the following inequality:

$$538 \quad \left[ \max_{x \in \Phi_a} \left\{ \log_2 \left( \frac{P_{\text{rx}}^2(x, o)}{P_{\text{rx}}^2(x, e^*(x))} \right) \right\} \right]^+ \geq \left[ \log_2 \left( \frac{P_{\text{rx}}^2(x_0, o)}{P_{\text{rx}}^2(x_0, e^*(x_0))} \right) \right]^+. \quad (28)$$

539 In other words, choosing the nearest AP to serve the legitimate  
540 user is sub-optimal, which gives an upper bound on the CDF  
541 of the secrecy capacity. Therefore, the upper bound expression  
542 shown in (25) can be obtained directly from Theorem 1. ■

543 Based on the upper bound on the CDF of the secrecy rate,  
544 a lower bound on the ergodic secrecy rate can be obtained,  
545 as given in (17). An upper bound on the ergodic secrecy  
546 rate can be obtained by integrating the complement of the  
547 CDF of  $R_s$ :

$$548 \quad \begin{aligned} 549 \quad \mathbb{E}[R_s] &= \int_0^\infty (1 - F_{R_s}(v)) dv \\ 550 &\leq \frac{m+3}{\ln(4)} \int_1^\infty \left( 1 - \exp \left( -\frac{\lambda_a}{\lambda_e \beta} \exp \left( -\pi \lambda_e (\beta-1) L^2 \right) \right) \right) \frac{1}{\beta} d\beta. \end{aligned} \quad (29)$$

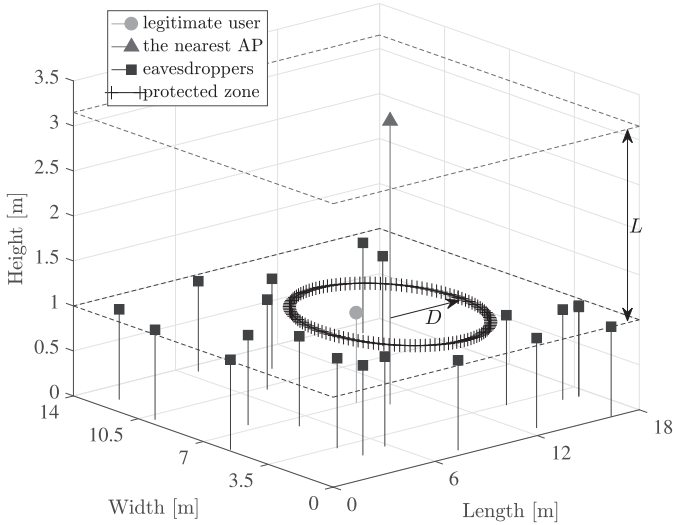


Fig. 2. Random network model with a secrecy protected zone. In this model, each VLC AP has a disk-shaped protected zone, which is centered around the AP and has a radius of  $D$  on the user plane. For simplicity, only the protected zone around the nearest AP is drawn.

Because of the nested exponential function in (29), a closed-form expression is not available. However, (29) can be efficiently calculated using numerical methods.

#### IV. ENHANCING SECRECY RATE IN VLC NETWORKS WITH A PROTECTED ZONE

In order to further enhance the secrecy performance of legitimate users in VLC networks, a strategy named the “protected zone” [34] can be implemented. As depicted in Fig. 2, a protected zone is an eavesdropper-free area (on the user plane), which allows only legitimate users to enter. If any eavesdropper enters the protected zone, such behavior will be made aware to the AP, and the AP will notify the legitimate user and temporarily stop the communication. A practical implementation of the protected zone in VLC networks can be achieved with motion sensors that are already built in modern energy-efficient lighting devices. We acknowledge that there might be means to break the suggested enforcement of the protected zone. However, a deeper investigation of this aspect is outside the scope of this work. A secrecy protected zone can be completely described by its center, i.e., its associated AP, and a security radius  $D$ . The security radius is defined as the smallest horizontal distance between the AP and any eavesdroppers that are undetectable.

*Lemma 1:* Given that the horizontal distance between the nearest AP to the legitimate user is  $x_0$ , the PDF of the horizontal distance between this AP and the nearest eavesdropper, that is outside the protected zone, is:

$$f_{\|e^*(x_0)-x_0\|}(\alpha) = 2\pi\lambda_e\alpha \exp\left(-\pi\lambda_e(\alpha^2 - D^2)\right), \quad (30)$$

for  $\alpha \geq D$ , and zero otherwise.

*Proof:* (30) can be obtained using the void probability of PPP [32]. ■

With Lemma 1, we are ready to obtain the CDF of the secrecy rate enhanced by the protected zone.

*Corollary 5:* When the legitimate user is served by the nearest AP in its vicinity, which has a protected zone with radius  $D$ , the CDF of the enhanced secrecy rate is given by:

$$F_{R_s}(v) = 1 - \frac{\exp\left(-\pi\lambda_e\left(\left(4^{\frac{v}{m+3}} - 1\right)L^2 - D^2\right)\right)}{1 + \frac{\lambda_e}{\lambda_a}4^{\frac{v}{m+3}}}, \quad (31)$$

for  $v \geq \frac{m+3}{2} \log_2(D^2/L^2 + 1)$ , and

$$F_{R_s}(v) = \frac{\exp\left(-\pi\lambda_a\left(D^2 - \left(4^{\frac{v}{m+3}} - 1\right)L^2\right)4^{-\frac{v}{m+3}}\right)}{1 + \frac{\lambda_a}{\lambda_e}4^{-\frac{v}{m+3}}}, \quad (32)$$

for  $0 \leq v < \frac{m+3}{2} \log_2(D^2/L^2 + 1)$ .

*Proof:* Since the protected zone has a radius  $D$ , the minimum distance between the nearest eavesdropper and the AP is  $D$ . Therefore,

$$e^*(x_0) = \arg \min_{e \in \Phi_e, e \notin \mathcal{B}(x_0, D)} \|e - x_0\|, \quad (33)$$

where  $\mathcal{B}(x_0, D)$  denotes the disk-shaped area centered at  $x_0$  with radius  $D$ . Due to the exclusive region in (33), the derivation of the CDF of the enhanced secrecy rate needs to be separated into two scenarios. First, when  $\sqrt{(\beta-1)L^2} \geq D$ , i.e.,  $v \geq \frac{m+3}{2} \log_2(D^2/L^2 + 1)$ , the CDF of the enhanced secrecy rate can be calculated as:

$$F_{R_s}(v) = \int_0^\infty \left(1 - \exp\left(-\pi\lambda_e\left(\beta x_0^2 + (\beta-1)L^2 - D^2\right)\right)\right) \times 2\pi\lambda_a x_0 \exp\left(-\pi\lambda_a x_0^2\right) dx_0, \quad (34)$$

which gives the result in (31). Second, when  $\sqrt{(\beta-1)L^2} < D$ , i.e.,  $0 \leq v < \frac{m+3}{2} \log_2(D^2/L^2 + 1)$ , the CDF of the enhanced secrecy rate can be calculated as:

$$F_{R_s}(v) = \int_{\sqrt{\frac{D^2 - (\beta-1)L^2}{\beta}}}^\infty 2\pi\lambda_a x_0 \exp\left(-\pi\lambda_a x_0^2\right) \times \left(1 - \exp\left(-\pi\lambda_e\left(\beta x_0^2 + (\beta-1)L^2 - D^2\right)\right)\right) dx_0 + \int_0^{\sqrt{\frac{D^2 - (\beta-1)L^2}{\beta}}} 2\pi\lambda_a x_0 \exp\left(-\pi\lambda_a x_0^2\right) \times \mathbb{P}\left[e^*(x_0) \in \mathcal{B}(x_0, D)\right] dx_0, \quad (35)$$

in which the critical point  $x_0 = \sqrt{(D^2 - (\beta-1)L^2)/\beta}$  is found by solving  $\sqrt{\beta x_0^2 + (\beta-1)L^2} = D$ . Since  $e^*(x_0) \notin \mathcal{B}(x_0, D)$ ,  $\mathbb{P}\left[e^*(x_0) \in \mathcal{B}(x_0, D)\right] = 0$ , and the second integration in (35) reduces to zero. After calculating the first integration in (35), we obtain (32). To this end, the proof is completed. ■

It can be seen from Corollary 5 that the radius of the protected zone has a strong impact on the CDF of the secrecy rate and on the secrecy outage probability. On the one hand, if the radius of the protected zone is small enough so that the target secrecy rate satisfies  $\bar{R}_s \geq \frac{m+3}{2} \log_2(D^2/L^2 + 1)$ , given a fixed density of eavesdroppers, the secrecy outage probability is lower bounded by:

$$P_{so}^{LB} = 1 - \exp\left(-\pi\lambda_e\left(\left(4^{\frac{\bar{R}_s}{m+3}} - 1\right)L^2 - D^2\right)\right), \quad (36)$$

629 which is obtained when the density of the APs goes to  
 630 infinity. On the other hand, if the radius of the protected  
 631 zone is large enough so that the target secrecy rate satisfies  
 632  $\bar{R}_s < \frac{m+3}{2} \log_2(D^2/L^2 + 1)$ , increasing the density of VLC  
 633 APs can efficiently reduce the secrecy outage probability, and  
 634 the worst-case scenario of the secrecy outage probability is  
 635 upper bounded by:

$$636 \quad p_{\text{so}}^{\text{UB}} = \exp\left(-\pi \lambda_a \left(D^2 - \left(4^{\frac{\bar{R}_s}{m+3}} - 1\right) L^2\right) 4^{-\frac{\bar{R}_s}{m+3}}\right), \quad (37)$$

637 which is obtained by letting  $\lambda_e$  approach infinity.

638 Corollary 5 provides an essential guideline to network  
 639 designers so that they can design a suitable protected zone  
 640 around each VLC AP in order to provide legitimate users  
 641 with guaranteed secrecy service. Specifically, for legitimate  
 642 users to achieve a target secrecy rate  $\bar{R}_s$  with a target  
 643 secrecy outage probability  $\bar{p}_{\text{so}}$ , network designers can set up  
 644 the protected zone with radius no smaller than  $D^*$ , where  
 645  $D^* = ((4^{\bar{R}_s/(m+3)} - 1)L^2 + (\ln(1 - \bar{p}_{\text{so}}) + \ln(1 + 4^{\bar{R}_s/(m+3)} \lambda_e/\lambda_a)) / \pi \lambda_e)^{1/2}$  for  $\bar{p}_{\text{so}} \geq 1 - (1 + 4^{\bar{R}_s/(m+3)} \lambda_e/\lambda_a)^{-1}$ ,  
 646 and  $D^* = ((4^{\bar{R}_s/(m+3)} - 1)L^2 - (\ln \bar{p}_{\text{so}} + \ln(1 + 4^{-\bar{R}_s/(m+3)} \lambda_a/\lambda_e)) / \pi \lambda_a)^{1/2}$  for  $\bar{p}_{\text{so}} < 1 - (1 + 4^{\bar{R}_s/(m+3)} \lambda_e/\lambda_a)^{-1}$ . Also, it is evident that a more stringent  
 647 secrecy requirement with a larger  $\bar{R}_s$  and/or a smaller  $\bar{p}_{\text{so}}$   
 648 requires the implementation of a larger secrecy protected zone.

649 *Theorem 3:* When the legitimate user is served by the  
 650 nearest AP in its vicinity, which has a protected zone with  
 651 radius  $D$ , the enhanced ergodic secrecy rate at the typical  
 652 legitimate user is:

$$656 \quad \mathbb{E}[R_s] \\
 657 = \frac{m+3}{\ln(4)} \left[ -\exp(\pi \lambda_e (L^2 + D^2)) \text{Ei}(-\pi \lambda_e (L^2 + D^2)) \right. \\
 658 \quad \left. + \ln\left(\frac{D^2}{L^2} + 1\right) \right] + \frac{m+3}{\ln(4)} \exp(\pi \lambda_a L^2) \left[ \text{Ei}(-\pi \lambda_a L^2) \right. \\
 659 \quad \left. + \exp(\pi \lambda_e (L^2 + D^2)) \text{Ei}(-\pi(\lambda_a + \lambda_e)(L^2 + D^2)) \right. \\
 660 \quad \left. - \text{Ei}(-\pi \lambda_a (L^2 + D^2)) \right]. \quad (38)$$

661 *Proof:* Based on Corollary 5, the enhanced ergodic rate  
 662 can be calculated by integrating the complement of the CDF.  
 663 Since the CDF has different expressions at different regions,  
 664 the integration should be separated into two parts:

$$665 \quad \mathbb{E}[R_s] \\
 666 = \frac{m+3}{\ln(4)} \int_1^{\frac{D^2}{L^2}+1} \left( 1 - \frac{\exp\left(\frac{-\pi \lambda_a (D^2 - (\beta-1)L^2)}{\beta}\right)}{1 + \frac{\lambda_a}{\lambda_e} \frac{1}{\beta}} \right) \frac{1}{\beta} d\beta \\
 667 + \frac{m+3}{\ln(4)} \int_{\frac{D^2}{L^2}+1}^{\infty} \frac{\exp(-\pi \lambda_e ((\beta-1)L^2 - D^2))}{\beta + \frac{\lambda_a}{\lambda_e} \beta^2} d\beta, \quad (39)$$

668 where for simplicity the variable of integration has been  
 669 changed from  $v$  to  $\beta$ . The first integration in (39) can be

simplified to:

$$670 \quad \int_1^{\frac{D^2}{L^2}+1} \left( 1 - \frac{\exp\left(\frac{-\pi \lambda_a (D^2 - (\beta-1)L^2)}{\beta}\right)}{1 + \frac{\lambda_a}{\lambda_e} \frac{1}{\beta}} \right) \frac{1}{\beta} d\beta \\
 671 \\
 672 = \ln\left(\frac{D^2}{L^2} + 1\right) + \exp(\pi \lambda_a L^2) \\
 673 \quad \times \int_1^{\frac{D^2}{L^2}+1} \frac{\exp\left(\frac{-\pi \lambda_a (L^2 + D^2)}{\beta}\right)}{\beta + \frac{\lambda_a}{\lambda_e}} d\beta, \quad (40)$$

in which the integration part can be obtained as:

$$674 \quad \int_1^{\frac{D^2}{L^2}+1} \frac{\exp\left(\frac{-\pi \lambda_a (L^2 + D^2)}{\beta}\right)}{\beta + \frac{\lambda_a}{\lambda_e}} d\beta \\
 675 \\
 676 = \text{Ei}(-\pi \lambda_a L^2) - \text{Ei}(-\pi \lambda_a (L^2 + D^2)) \\
 677 \quad + \exp(\pi \lambda_e (L^2 + D^2)) \text{Ei}(-\pi(\lambda_a + \lambda_e)(L^2 + D^2)) \\
 678 \quad - \exp(\pi \lambda_e (L^2 + D^2)) \text{Ei}(-\pi \lambda_a L^2 - \pi \lambda_e (L^2 + D^2)). \\
 679 \quad (41)$$

Similarly, the second integration in (39) can be simplified to:

$$680 \quad \int_{\frac{D^2}{L^2}+1}^{\infty} \frac{\exp(-\pi \lambda_e ((\beta-1)L^2 - D^2))}{\beta + \frac{\lambda_a}{\lambda_e} \beta^2} d\beta \\
 681 \\
 682 = \exp(\pi \lambda_e (L^2 + D^2)) \left[ \int_{\frac{D^2}{L^2}+1}^{\infty} \frac{\exp(-\pi \lambda_e \beta L^2)}{\beta} d\beta \right. \\
 683 \quad \left. - \int_{\frac{D^2}{L^2}+1}^{\infty} \frac{\exp(-\pi \lambda_e \beta L^2)}{\beta + \frac{\lambda_a}{\lambda_e}} d\beta \right]. \quad (42)$$

684 Applying [33, eq. 3.352.2], the two integrations in (42) can  
 685 be calculated as:

$$686 \quad \int_{\frac{D^2}{L^2}+1}^{\infty} \frac{\exp(-\pi \lambda_e \beta L^2)}{\beta} d\beta = -\text{Ei}(-\pi \lambda_e (L^2 + D^2)), \quad (43)$$

and

$$687 \quad \int_{\frac{D^2}{L^2}+1}^{\infty} \frac{\exp(-\pi \lambda_e \beta L^2)}{\beta + \frac{\lambda_a}{\lambda_e}} d\beta \\
 688 \\
 689 = -\exp(\pi \lambda_a L^2) \text{Ei}\left(-\pi \lambda_e L^2 \left(\frac{\lambda_a}{\lambda_e} + \frac{D^2}{L^2} + 1\right)\right). \quad (44)$$

690 Combining (40) – (44) gives the result shown in (38), which  
 691 completes the proof. ■

692 Note that the expression for the ergodic secrecy rate  
 693 in Theorem 3 can be simplified to the one given in Theorem 2  
 694 when  $D = 0$ . Also, it is shown in Theorem 3 that the ergodic  
 695 secrecy rate scales linearly with the Lambertian order  $m$ ,  
 696 regardless of the size of the protected zone. Given the choice  
 697 of LEDs, the density of APs and the density of eavesdroppers,  
 698 a target ergodic secrecy capacity  $\bar{R}_s$  can be achieved through  
 699 the implementation of a protected zone with radius  $D^*$ , where

TABLE I  
SIMULATION PARAMETERS

Parameter	value
Room dimensions	$18 \times 14 \times 3.5 \text{ m}^3$
Height of VLC APs	3.15 m
Height of mobile users	1 m
Semi-angle of VLC APs, $\Phi_{1/2}$	$30^\circ$
Transmit optical power of VLC APs, $P_{\text{tx}}$	1 W
Receiver detection area, $A$	$1 \text{ cm}^2$
Receiver responsivity, $\eta$	0.4 A/W
Reflective index of the optical concentrator, $n$	1.5
Optical filter gain, $T$	1
Receiver FOV, $\Psi_{\text{fov}}$	$90^\circ$
Receiver noise power, $\sigma_{\text{nb}}^2 = \sigma_{\text{nc}}^2$	-103.98 dBm

700  $D^*$  is the numerical solution for  $D$  by letting (38) equal  $\bar{R}_s$ .  
 701 Since the expression in (38) monotonically increases with  
 702 respect to  $D$ , the numerical solution for  $D^*$  is unique.

## V. SIMULATION RESULTS AND DISCUSSIONS

### A. Results Based on the PPP Model

705 In this section, we use a MATLAB implementation to  
 706 validate the derived results. Simulation results are obtained  
 707 by averaging 20,000 realizations of Monte Carlo simulations.  
 708 A typical office of size  $18 \times 14 \times 3.5 \text{ m}^3$  is considered,  
 709 as illustrated in Figs. 1 and 2. If not otherwise specified,  
 710 the network parameters used for the simulation setup are  
 711 described in Table I.

712 First, we consider the scenario where the legitimate user is  
 713 served by the nearest AP in its vicinity, without the imple-  
 714 mentation of the secrecy protected zone. Therefore, malicious  
 715 eavesdroppers can be horizontally as close as possible to the  
 716 AP that serves the legitimate user. By fixing the density of  
 717 eavesdroppers ( $\lambda_e = 0.2$ ), the secrecy outage probability at  
 718 the typical legitimate user is evaluated at different values of  
 719 the AP density, as shown in Fig. 3. It can be seen that,  
 720 when  $\lambda_a$  is small, increasing the density of VLC APs can  
 721 efficiently reduce the secrecy outage probability at the legiti-  
 722 mate user. However, when  $\lambda_a$  is large, further increasing the  
 723 density of VLC APs only slightly reduces the secrecy outage  
 724 probability. For example, given that the target secrecy rate is  
 725  $\bar{R}_s = 1 \text{ bit/s/Hz}$ , increasing  $\lambda_a$  from 0.1 to 1 can cause the  
 726 secrecy outage probability to drop by 0.3. In comparison, when  
 727  $\lambda_a$  is increased from 1 to 10, the secrecy outage probability  
 728 only drops by 0.1. Also, it is shown that a lower bound on  
 729 the secrecy outage probability exists even if the density of  
 730 VLC APs approaches infinity. This result is in agreement  
 731 with Corollary 2. In Fig. 4, the ergodic secrecy rate is plotted  
 732 against the density of APs. It is shown that the ergodic secrecy  
 733 rate at the legitimate user drops when the density of eaves-  
 734 droppers increases. Given a fixed density of eavesdroppers,  
 735 increasing the density of VLC APs can efficiently enhance the  
 736 ergodic secrecy rate when  $\lambda_a$  is small. However, the ergodic  
 737 secrecy rate of the legitimate user tends to saturate at high  
 738 AP densities. As a result, increasing the density of VLC APs  
 739 when  $\lambda_a$  is large does not bring a significant incrementation  
 740 to the ergodic secrecy rate. Instead, increasing the density of  
 741 APs when  $\lambda_a$  is small is more meaningful.

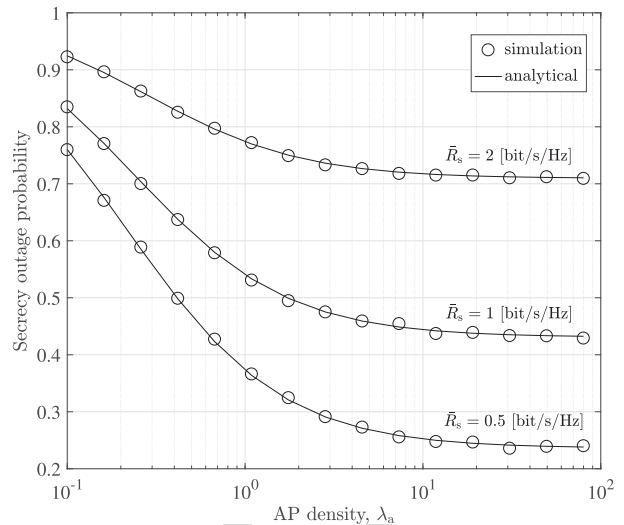


Fig. 3. Secrecy outage probability versus VLC AP density. The legitimate user is served by the nearest AP in its vicinity.  $\lambda_e = 0.2$ .

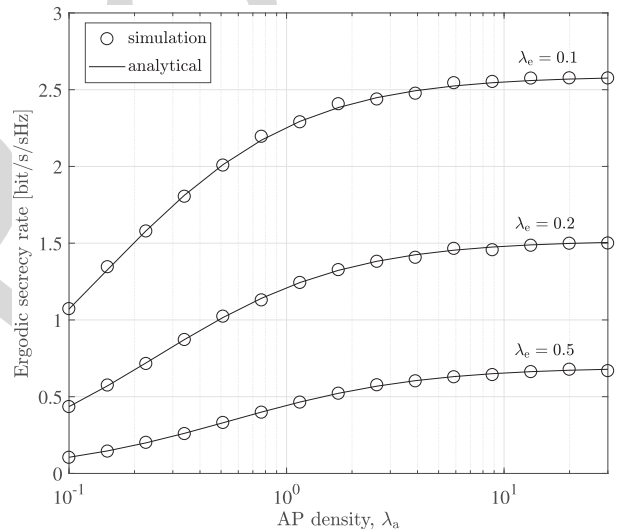


Fig. 4. Ergodic secrecy rate versus VLC AP density. The legitimate user is served by the nearest AP in its vicinity.

742 Second, we consider the scenario where the legitimate user  
 743 is served by the optimal AP when APs are cooperated in the  
 744 network. For the typical legitimate user, the optimal AP is  
 745 not necessarily the nearest one, depending on the locations  
 746 of potential eavesdroppers. With the cooperation among VLC  
 747 APs, the optimal AP that brings the highest secrecy rate to  
 748 the legitimate user is selected. For Monte Carlo simulations,  
 749 the optimal AP is found out through the exhaustive search  
 750 method. In Fig. 5, the secrecy outage probability is plotted  
 751 against different eavesdropper densities, and it can be seen  
 752 that the simulation results are well bounded by the derived  
 753 analytical results. On the one hand, by assuming that the  
 754 optimal AP is the nearest one, we underestimate the secrecy  
 755 rate at the legitimate user. As a result, this assumption leads to  
 756 an upper bound on the secrecy outage probability. On the other  
 757 hand, the lower bound on the secrecy outage probability is

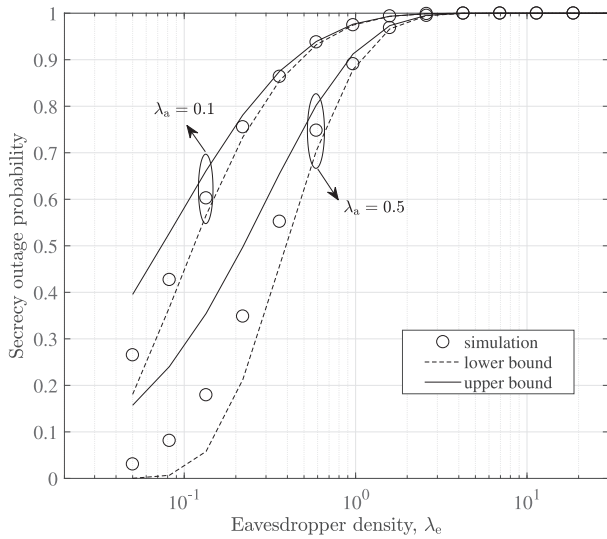


Fig. 5. Secrecy outage probability versus eavesdropper density. The legitimate user is served by the optimal AP.  $\bar{R}_s = 0.5$  bit/s/Hz.

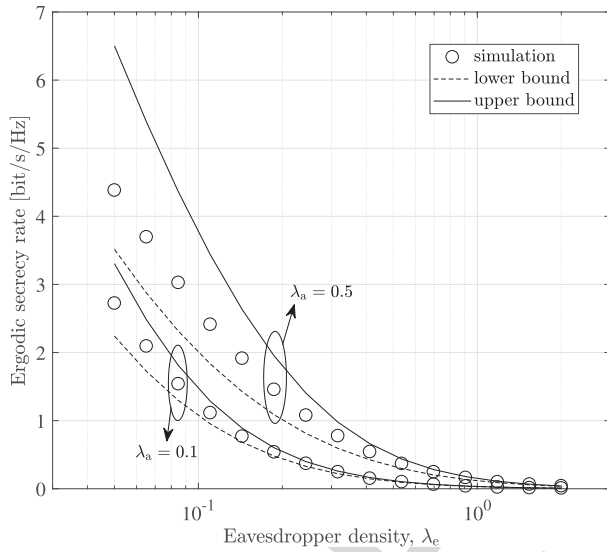


Fig. 6. Ergodic secrecy rate versus eavesdropper density. The legitimate user is served by the optimal AP.

obtained from Jensen's inequality, as described in Corollary 4. Comparing the lower bound with the upper bound, it can be seen that the lower bound is closer to the simulation results. It is also shown in Fig. 5 that both theoretical bounds on the secrecy outage probability are reasonably tight when the eavesdropper density is large. In Fig. 6, the ergodic secrecy rate at the legitimate user is computed for different values of the eavesdropper density. It should be noted that assuming the optimal AP is the nearest one gives the lower bound on the ergodic secrecy rate in Fig. 6, which corresponds to the upper bound on the secrecy outage probability in Fig. 5. Again, both analytical bounds become tighter as the eavesdropper density increases. Based on the results shown in Fig. 5 and Fig. 6, we can conclude that the optimal AP that maximizes the secrecy performance at the legitimate user is not necessarily the nearest one. To investigate deeper, we show in Fig. 7

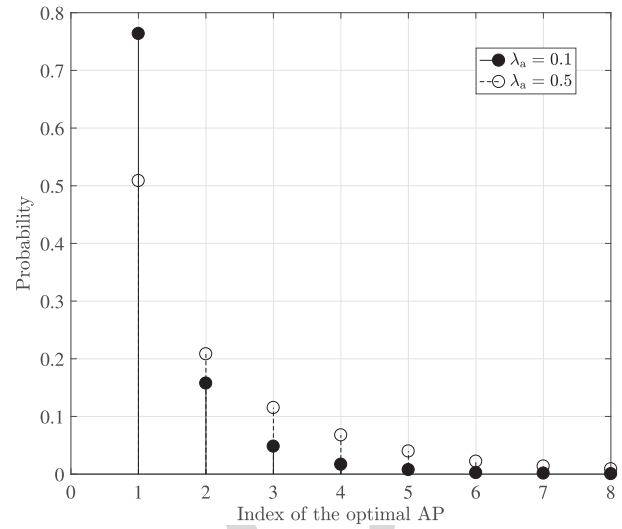


Fig. 7. Probability mass function (PMF) of the index of the optimal AP.  $\lambda_e = 0.2$ .

the probability mass function (PMF) of the index of the optimal AP that maximizes the secrecy rate at the legitimate user. Index  $i$  relates to the  $i$ -th nearest neighboring AP to the legitimate user. For example, index 1 corresponds to the nearest AP, index 2 corresponds to the second nearest AP, and so on. It is shown in Fig. 7 that, compared to other neighboring APs, the nearest AP is most likely the optimal one. However, it is also possible that the optimal AP is the second nearest, third nearest, etc. Fig. 7 also shows that with a smaller value of  $\lambda_a$ , it is more likely that the nearest AP is the optimal one, which therefore explains why the analytical bounds are tighter for smaller values of  $\lambda_a$ , as observed in Fig. 5 and Fig. 6.

Third, we consider the scenario where the legitimate user is served by the nearest AP in its vicinity, with the implementation of a secrecy protected zone. It is assumed that any malicious eavesdroppers that are inside the protected zone can be detected by the AP so that these eavesdroppers do not cause any secrecy information loss at the legitimate user. As a result, the secrecy information loss at the legitimate user is caused by the eavesdroppers that are outside the protected zone only. In Fig. 8, the secrecy outage probability is plotted against the density of VLC APs. It is shown that, for a given target secrecy rate, the secrecy outage probability decreases as the AP density increases. However, when  $\lambda_a$  is large, further increasing the density of VLC APs only slightly reduces the secrecy outage probability. Also, it is shown that there exists a lower bound on the secrecy outage probability when  $\lambda_a$  approaches infinity. After implementing a secrecy protected zone with radius  $D$ , the secrecy outage probability is reduced significantly. More specifically, when  $\lambda_a = 1$ ,  $\lambda_e = 0.2$  and the target secrecy rate is  $\bar{R}_s = 2$  bit/s/Hz, implementing a secrecy protected zone with radius  $D = 1$  m reduces the secrecy outage probability by 0.2. If the secrecy protected zone has a radius of  $D = 2$  m, the secrecy outage probability can be reduced to nearly zero. It is also shown in Fig. 8 that, with a sufficiently large protected area, the secrecy outage probability is no longer bounded at the lower end, i.e., increasing the density of VLC



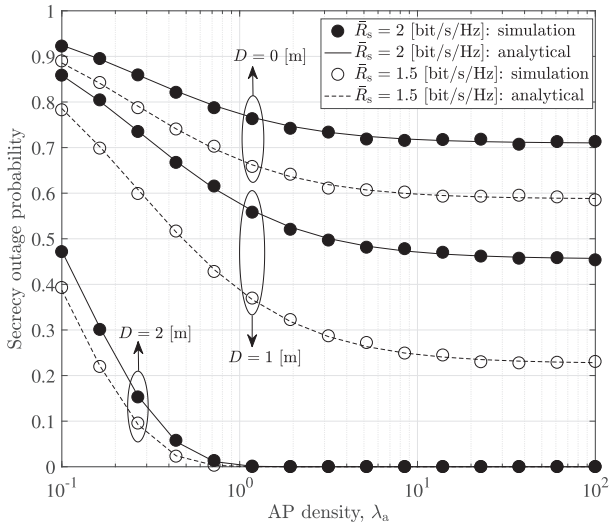


Fig. 8. Secrecy outage probability versus VLC AP density. The legitimate user is served by the nearest AP in its vicinity, and eavesdroppers are outside the protected zone with radius  $D$ .  $\lambda_e = 0.2$ .

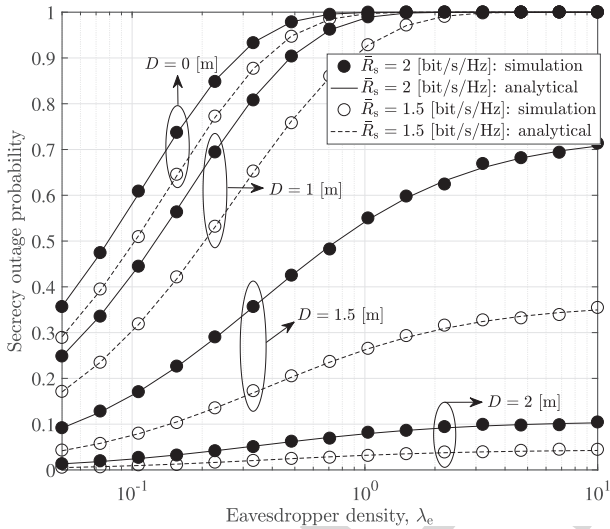


Fig. 9. Secrecy outage probability versus eavesdropper density. The legitimate user is served by the nearest AP in its vicinity, and eavesdroppers are outside the protected zone with radius  $D$ .  $\lambda_a = 0.5$ .

811 APs can efficiently reduce the secrecy outage probability to  
 812 zero. In Fig. 9, we fix  $\lambda_a = 0.5$  and evaluate the impact of  
 813 the eavesdropper density on the secrecy outage probability.  
 814 It can be seen that, without the protected zone, the secrecy  
 815 outage probability can be as large as one if the eavesdropper  
 816 density is sufficiently high. However, with the implementa-  
 817 tion of a protected zone, the worst-case scenario of the secrecy  
 818 outage probability can be limited below a certain level. For  
 819 example, when the target secrecy rate is  $\bar{R}_s = 2$  bit/s/Hz and  
 820 the protected zone has a radius of  $D = 2$  m, the worst-case  
 821 secrecy outage probability at the legitimate user does not  
 822 exceed 0.12, regardless of the eavesdropper density. To fur-  
 823 ther investigate the impact of the protected zone, we show  
 824 in Fig. 10 the ergodic secrecy rate against the radius of the  
 825 protected zone while fixing the eavesdropper density to  
 826  $\lambda_e = 0.2$ . The slope of the curve shows that a very small  
 827 protected area brings only marginal improvement on the

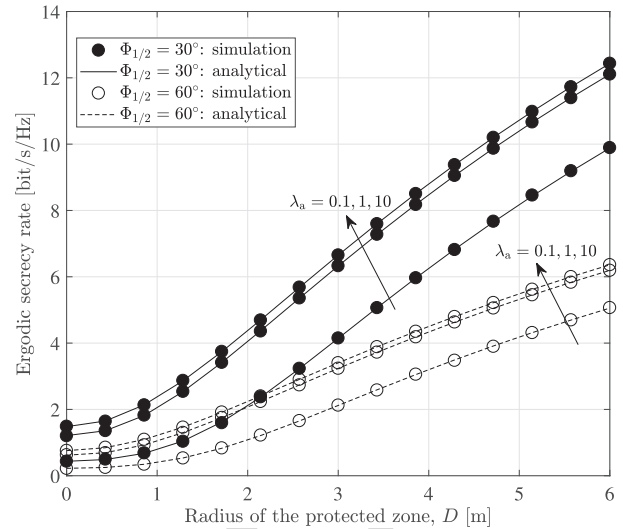


Fig. 10. Ergodic secrecy rate versus the radius of the protected zone. The legitimate user is served by the nearest AP in its vicinity.  $\lambda_e = 0.2$ .

828 secrecy performance. However, by increasing the size of  
 829 the protected zone further, the secrecy performance at the  
 830 legitimate user can be enhanced significantly. Specifically,  
 831 when  $\lambda_a = 1$  and  $\Phi_{1/2} = 30^\circ$ , increasing the radius of the  
 832 protected zone from 0 to 1 m increases the ergodic secrecy  
 833 rate by 0.6 bit/s/Hz. In contrast, increasing the radius of  
 834 the protected zone from 1 to 2 m can increase the ergodic  
 835 secrecy rate by 1.9 bit/s/Hz. In Fig. 10, it is also shown that  
 836 using more directional LEDs, i.e., LEDs with a smaller semi-  
 837 angle, enhances the secrecy performance at the legitimate user.  
 838 However, the actual choice of LEDs should also take practical  
 839 illumination requirements into consideration.

840 **B. PPP Model vs. Grid Model**

841 In the following, we compare the secrecy performance  
 842 between the stochastic PPP model and the deterministic grid  
 843 model. For the grid model, it implicitly assumes that the  
 844 number of APs, as well as their locations in the network, are  
 845 fixed and known. As shown in Fig. 11 and Fig. 12, we use a  
 846 hexagonal-shaped grid to model the locations of APs within  
 847 the same indoor space. A total number of 31 APs (represented  
 848 by red triangles) are considered, and without loss of generality  
 849 the secrecy performance is studied by focusing on the central  
 850 hexagonal cell. A legitimate user (represented by the green  
 851 circle) is randomly distributed within the central cell and is  
 852 served by the central AP. The eavesdroppers (represented by  
 853 blue squares) are assumed to follow a Poisson distribution  
 854 with intensity  $\lambda_e$ . To allow for a fair comparison between  
 855 the PPP model and the grid model, the density of APs in  
 856 the PPP model is set to 0.12 so that the expected number  
 857 of APs in the PPP model equals the total number of APs  
 858 in the grid model. It can be seen from Fig. 11 that the  
 859 PPP model and the grid model yield similar results for the  
 860 secrecy outage probability. Both curves have similar shapes  
 861 and trends, especially for higher target secrecy rates and  
 862 with larger eavesdropper densities. In general, the grid model

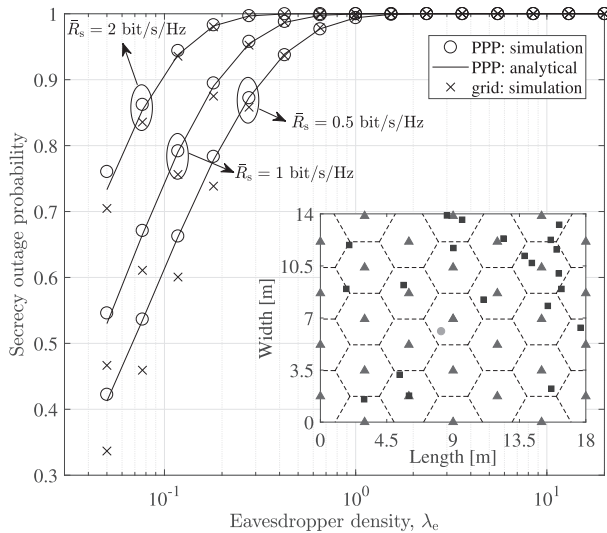


Fig. 11. Secrecy outage probability comparison between the PPP model and the grid model.  $\lambda_a = 0.12$ .

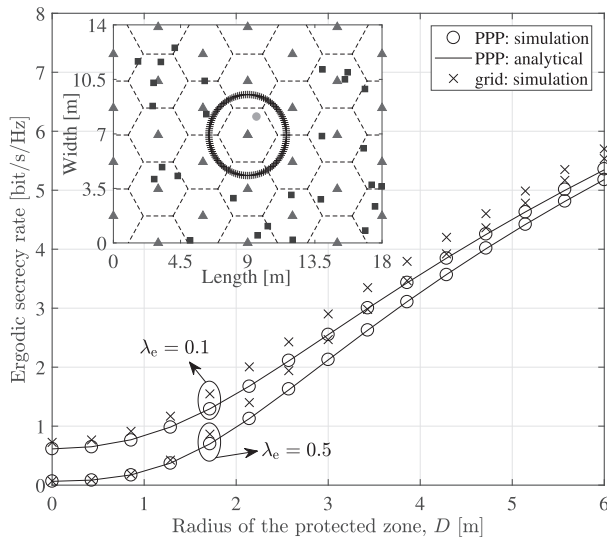


Fig. 12. Ergodic secrecy rate comparison between the PPP model and the grid model.  $\lambda_a = 0.12$ .

provides slightly superior coverage performance than the PPP model because of its more regularized cell shapes. With the implementation of a secrecy protected zone, we compare in Fig. 12 the achieved ergodic secrecy rate between the PPP model and the grid model. The configuration of the grid model in Fig. 12 is the same as that in Fig. 11, except that the eavesdroppers are prohibited in the circular protected zone centered around the central AP. Results show that both models yield close ergodic secrecy rates, especially for networks with more populated eavesdroppers.

## VI. CONCLUSION

In this work, we studied the performance of physical-layer secrecy in a three-dimensional multiuser VLC network. With the use of mathematical tools from stochastic geometry, analytical expressions for the secrecy outage probability, the ergodic secrecy rate, as well as their lower and upper bounds, are

derived in tractable forms and verified through Monte Carlo simulations. Impacts of AP cooperation and the implementation of a secrecy protected zone on the secrecy performance have also been investigated. Results show that cooperating neighboring APs can enhance the secrecy performance of VLC networks, but only to a limited extent. We also show that building a secrecy protected zone around the AP significantly improves the network secrecy performance.

Justifying the application of the PPP model to the performance analysis of VLC networks is an important research direction. Also, improved stochastic models may be developed in the future to more accurately capture the spatial distribution of APs in a real network deployment.

## REFERENCES

- [1] T. Komine and M. Nakagawa, "Fundamental analysis for visible-light communication system using LED lights," *IEEE Trans. Consum. Electron.*, vol. 50, no. 1, pp. 100–107, Feb. 2004.
- [2] S. Dimitrov and H. Haas, *Principles of LED Light Communications: Towards Networked Li-Fi*. Cambridge, U.K.: Cambridge Univ. Press, 2015.
- [3] H. Haas, L. Yin, Y. Wang, and C. Chen, "What is Li-Fi?" *J. Lightw. Technol.*, vol. 34, no. 6, pp. 1533–1544, Mar. 15, 2016.
- [4] *IEEE Standard for Local and Metropolitan Area Networks—Part 15.7: Short-Range Wireless Optical Communication Using Visible Light*, IEEE Computer Society, IEEE Standard 802.15.7-2011, 2011.
- [5] X. Li, F. Jin, R. Zhang, J. Wang, Z. Xu, and L. Hanzo, "Users first: User-centric cluster formation for interference-mitigation in visible-light networks," *IEEE Trans. Wireless Commun.*, vol. 15, no. 1, pp. 39–53, Jan. 2016.
- [6] H. Ma, L. Lampe, and S. Hranilovic, "Coordinated broadcasting for multiuser indoor visible light communication systems," *IEEE Trans. Commun.*, vol. 63, no. 9, pp. 3313–3324, Sep. 2015.
- [7] L. Yin, W. O. Popoola, X. Wu, and H. Haas, "Performance evaluation of non-orthogonal multiple access in visible light communication," *IEEE Trans. Commun.*, vol. 64, no. 12, pp. 5162–5175, Dec. 2016.
- [8] A. D. Wyner, "The wire-tap channel," *Bell Syst. Tech. J.*, vol. 54, no. 8, pp. 1355–1387, 1975.
- [9] I. Csiszár and J. Körner, "Broadcast channels with confidential messages," *IEEE Trans. Inf. Theory*, vol. IT-24, no. 3, pp. 339–348, May 1978.
- [10] M. Haenggi, "The secrecy graph and some of its properties," in *Proc. IEEE Int. Symp. Inf. Theory*, Toronto, ON, Canada, Jul. 2008, pp. 539–543.
- [11] P. C. Pinto, J. Barros, and M. Z. Win, "Secure communication in stochastic wireless networks—Part I: Connectivity," *IEEE Trans. Inf. Forensics Security*, vol. 7, no. 1, pp. 125–138, Feb. 2012.
- [12] P. C. Pinto, J. Barros, and M. Z. Win, "Secure communication in stochastic wireless networks—Part II: Maximum rate and collusion," *IEEE Trans. Inf. Forensics Security*, vol. 7, no. 1, pp. 139–147, Feb. 2012.
- [13] O. O. Koyluoglu, C. E. Koksall, and H. El Gamal, "On secrecy capacity scaling in wireless networks," *IEEE Trans. Inf. Theory*, vol. 58, no. 5, pp. 3000–3015, May 2012.
- [14] X. Zhou, R. K. Ganti, J. G. Andrews, and A. Hjørungnes, "On the throughput cost of physical layer security in decentralized wireless networks," *IEEE Trans. Wireless Commun.*, vol. 10, no. 8, pp. 2764–2775, Aug. 2011.
- [15] H. Wang, X. Zhou, and M. C. Reed, "Physical layer security in cellular networks: A stochastic geometry approach," *IEEE Trans. Wireless Commun.*, vol. 12, no. 6, pp. 2776–2787, Jun. 2013.
- [16] A. Lapidath, S. M. Moser, and M. A. Wigger, "On the capacity of free-space optical intensity channels," *IEEE Trans. Inf. Theory*, vol. 55, no. 10, pp. 4449–4461, Oct. 2009.
- [17] J.-B. Wang, Q.-S. Hu, J. Wang, M. Chen, and J.-Y. Wang, "Tight bounds on channel capacity for dimmable visible light communications," *J. Lightw. Technol.*, vol. 31, no. 23, pp. 3771–3779, Dec. 1, 2013.
- [18] A. Chaaban, J. M. Morvan, and M. S. Alouini, "Free-space optical communications: Capacity bounds, approximations, and a new sphere-packing perspective," *IEEE Trans. Commun.*, vol. 64, no. 3, pp. 1176–1191, Mar. 2016.

- 948 [19] S. Dimitrov and H. Haas, "Information rate of OFDM-based optical  
949 wireless communication systems with nonlinear distortion," *J. Lightw.  
950 Technol.*, vol. 31, no. 6, pp. 918–929, Mar. 15, 2013.
- 951 [20] A. Mostafa and L. Lampe, "Physical-layer security for MISO visible  
952 light communication channels," *IEEE J. Sel. Areas Commun.*, vol. 33,  
953 no. 9, pp. 1806–1818, Sep. 2015.
- 954 [21] A. Mostafa and L. Lampe, "Optimal and robust beamforming for  
955 secure transmission in MISO visible-light communication links,"  
956 *IEEE Trans. Signal Process.*, vol. 64, no. 24, pp. 6501–6516,  
957 Dec. 2016.
- 958 [22] G. Pan, J. Ye, and Z. Ding, "On secure VLC systems with spatially  
959 random terminals," *IEEE Commun. Lett.*, vol. 21, no. 3, pp. 492–495,  
960 Mar. 2016.
- 961 [23] D. Stoyan, W. Kendall, and J. Mecke, *Stochastic Geometry and its  
962 Applications*, 2nd ed. Hoboken, NJ, USA: Wiley, 1996.
- 963 [24] L. Zeng *et al.*, "High data rate multiple input multiple output  
964 (MIMO) optical wireless communications using white LED light-  
965 ing," *IEEE J. Sel. Areas Commun.*, vol. 27, no. 9, pp. 1654–1662,  
966 Dec. 2009.
- 967 [25] J. Grubor, S. Randel, K. D. Langer, and J. W. Walewski, "Broadband  
968 information broadcasting using LED-based interior lighting," *J. Lightw.  
969 Technol.*, vol. 26, no. 24, pp. 3883–3892, Dec. 15, 2008.
- 970 [26] J. M. Kahn and J. R. Barry, "Wireless infrared communications," *Proc.  
971 IEEE*, vol. 85, no. 2, pp. 265–298, Feb. 1997.
- 972 [27] L. Hanzo, H. Haas, S. Imre, D. O'Brien, M. Rupp, and L. Gyongyosi,  
973 "Wireless myths, realities, and futures: From 3G/4G to optical and  
974 quantum wireless," *Proc. IEEE*, vol. 100, pp. 1853–1888, May 2012.
- 975 [28] C. Chen, S. Videv, D. Tsonev, and H. Haas, "Fractional frequency reuse  
976 in DCO-OFDM-based optical attocell networks," *J. Lightw. Technol.*,  
977 vol. 33, no. 19, pp. 3986–4000, Oct. 1, 2015.
- 978 [29] S. Leung-Yan-Cheong and M. E. Hellman, "The Gaussian wire-tap  
979 channel," *IEEE Trans. Inf. Theory*, vol. IT-24, no. 4, pp. 451–456,  
980 Jul. 1978.
- 981 [30] O. Ozel, E. Ekrem, and S. Ulukus, "Gaussian wiretap channel with  
982 an amplitude constraint," in *Proc. IEEE Inf. Theory Workshop (ITW)*,  
983 Sep. 2012, pp. 139–143.
- 984 [31] M. Haenggi, "On distances in uniformly random networks," *IEEE Trans.  
985 Inf. Theory*, vol. 51, no. 10, pp. 3584–3586, Oct. 2005.
- 986 [32] S. Srinivasa and M. Haenggi, "Distance distributions in finite uniformly  
987 random networks: Theory and applications," *IEEE Trans. Veh. Technol.*,  
988 vol. 59, no. 2, pp. 940–949, Feb. 2010.
- 989 [33] I. S. Gradshteyn and I. M. Ryzhik, *Tables of Integrals, Series, and  
990 Products*, 7th ed. San Diego, CA, USA: Academic, 2007.
- 991 [34] N. Romero-Zurita, D. McLernon, M. Ghogho, and A. Swami, "PHY  
992 layer security based on protected zone and artificial noise," *IEEE Signal  
993 Process. Lett.*, vol. 20, no. 5, pp. 487–490, May 2013.



**Liang Yin** received the B.Eng. degree (Hons.) in electronics and electrical engineering from the University of Edinburgh, Edinburgh, U.K., in 2014, where he is currently pursuing the Ph.D. degree in electrical engineering. His research interests are in visible light communication and positioning, multi-user networking, and wireless network performance analysis. He received the Class Medal Award and IET Prize Award from the University of Edinburgh.



**Harald Haas** (S'98–AM'00–M'03–SM'17) received the Ph.D. degree from the University of Edinburgh in 2001. He currently holds the Chair of mobile communications with the University of Edinburgh, and is the Initiator, Co-Founder, and the Chief Scientific Officer of pureLiFi Ltd and the Director of the LiFi Research and Development Center, University of Edinburgh. He has authored 400 conference and journal papers including a paper in Science and co-authored a book entitled *Principles of LED Light Communications Towards*

*Networked Li-Fi* (Cambridge University Press, 2015). His main research interests are in optical wireless communications, hybrid optical wireless and RF communications, spatial modulation, and interference coordination in wireless networks. He first introduced and coined spatial modulation and LiFi. LiFi was listed among the 50 best inventions in TIME Magazine 2011. He was an invited speaker with TED Global 2011, and his talk on Wireless Data from Every Light Bulb has been watched online over 2.4 million times. He gave a second TED Global lecture in 2015 on the use of solar cells as LiFi data detectors and energy harvesters. This has been viewed online over 1.8 million times. He was elected as a Fellow of the Royal Society of Edinburgh in 2017. In 2012 and 2017, he was the recipient of the prestigious Established Career Fellowship from the Engineering and Physical Sciences Research Council (EPSRC) within Information and Communications Technology in the U.K. In 2014, he was selected by EPSRC as one of ten Recognising Inspirational Scientists and Engineers Leaders in the U.K. He was the co-recipient of the EURASIP Best Paper Award for the *Journal on Wireless Communications and Networking* in 2015, and co-recipient of the Jack Neubauer Memorial Award of the IEEE VEHICULAR TECHNOLOGY SOCIETY. In 2016, he was a recipient of the outstanding achievement award from the International Solid State Lighting Alliance. He was the co-recipient of recent Best Paper Awards at VTC, 2013, VTC 2015, ICC 2016, and ICC 2017. He is currently an Editor of the IEEE TRANSACTIONS ON COMMUNICATIONS and the IEEE JOURNAL OF LIGHTWAVE TECHNOLOGIES.